Thiosemicarbazone(s)-anchored water soluble mono- and bimetallic Cu(II) complexes: Enzymes-like activities, biomolecular interactions, anticancer property and real-time live cytotoxicity

Nithya Balakrishnan, Jebiti Haribabu, Ananda Krishnan Dhanabalan, Srividya Swaminathan, Sijia Sun, Dya Fita Dibwe, Nattamai Bhuvanesh, Suresh Awale, Ramasamy Karvembu*

Experimental

Materials and methods

All the required chemicals, solvents and biomolecules were purchased from Sigma Aldrich / Merck. The melting points were determined on a Lab India instrument and are uncorrected. FT-IR spectra were obtained as KBr pellets using a Nicolet-iS5 spectrophotometer. UV-Visible spectra were recorded using a Shimadzu-2600 spectrophotometer. ^{1}H and ^{13}C NMR spectra were recorded in DMSO-d_6 by using TMS as an internal standard on a Bruker 400 or 100 MHz spectrometer respectively. X band EPR spectra were recorded on a JES-FA200 ESR spectrometer operating at 8.75-9.65 GHz magnetic field modulation at room temperature (RT) and liquid nitrogen temperature (LNT). High resolution mass spectra were recorded on a Bruker mass spectrometer. TGA were done from RT to 400°C at a heating rate of 10°C/min on a Shimadzu TGA-51 thermal analyser. The emission spectra of the compounds were obtained from Horiba spectrofluorometer equipped with xenon arc lamp.

Synthesis of the ligands (L1-L5)

The ligands were synthesized according to literature reports with slight modifications.[21,28] To an ethanolic solution of 4-oxo-4H-chromene-3-carbaldehyde (0.3 g, 1.75 mmol), an ethanolic solution of thiosemicarbazide / 4(*N*)-methylthiosemicarbazide / 4(*N*)-ethylthiosemicarbazide / 4(*N*)-cyclohexylthiosemicarbazide / 4(*N*)-phenylthiosemicarbazide (0.435-0.579 g, 1.75 mmol) was added. After the addition of 1-2 drops of acetic acid, the mixture was kept under reflux for 2 h. The white compound precipitated was collected by filtration, washed well with cold ethanol, and dried in *vacuum*. The yields and spectral data of the ligands were in line with the reported values.

4-oxo-4H-chromene-3-carbaldehydethiosemicarbazone (L1)

Yield: 96%. M.p.: 245°C. FT-IR (KBr): υ, cm^{-1} 3242 (N–H), 3151 (H–N–C=S), 1642 (C=O), 1600 (C=N), 841 (C=S). UV–Vis (DMF): λ_{max}, nm (ε, dm^{3}mol^{-1}cm^{-1}) 323 (11,850) (n→π*), 245 (12,850) (π→π*). ^{1}H NMR (400 MHz, DMSO-d$_6$): δ, ppm 11.55 (s, 1H, –N**H**–C=S), 9.15 (s, 1H, C**H**=N), 8.26 (s, 2H, –N**H**$_2$), 8.18 (s, 1H, C2–**H**), 8.11 (d, *J* = 9.5 Hz, 1H, C5–**H**),

7.84 (t, *J* = 10 Hz, 1H, C6–**H**), 7.71 (d, *J* = 10.5 Hz, 1H, C7–**H**), 7.54 (t, *J* = 9.5 Hz 1H, C8–**H**). ^{13}C NMR (100 MHz, DMSO-d_6): δ, ppm 178.49 (C=S), 175.31(C=O), 156.19 (C–O), 155.7 (C=N), 135.03, 134.61, 126.52, 125.63, 123.77, 119.19, 118.75 (aromatic carbons of chromone moiety).

4-oxo-4H-chromene-3-carbaldehyde-4(*N*)-methylthiosemicarbazone (L2)

Yield: 82%. M.p.: 262°C. FT-IR (KBr): υ, cm^{-1} 3351 (N–H), 3056 (H–N–C=S), 1632 (C=O), 1557 (C=N), 845 (C=S). UV–Vis (DMF): λ_{max}, nm (ε, $dm^3mol^{-1}cm^{-1}$) 321 (11,050) (n→π*), 245 (8,100) (π→π*). ^{1}H NMR (400 MHz, DMSO-d_6): δ, ppm 11.61 (s, 1H, –N**H**–C=S), 9.09 (s, 1H, C**H**=N), 8.58 (d, *J* = 5 Hz, 1H, terminal –N**H**), 8.16 (s, 1H, C2–**H**), 8.10 (d, *J* = 10 Hz, 1H, C5–**H**), 7.83 (t, *J* = 9 Hz, 1H, C6–**H**), 7.69 (d, *J* = 10.5 Hz, 1H, C7–**H**), 7.52 (t, *J* = 9.5 Hz, 1H, C8–**H**), 3.02 (d, *J* = 5 Hz, 3H, –C**H**$_3$). ^{13}C NMR (100 MHz, DMSO-d_6): δ, ppm 178.1 (C=S), 175.2 (C=O), 156.1 (C–O), 155.3 (C=N), 134.9, 133.9, 126.4, 204, 125.6, 123.7, 119.1, 118.8 (aromatic carbons of chromone moiety), 31.1 (CH_3).

4-oxo-4H-chromene-3-carbaldehyde-4(*N*)-ethylthiosemicarbazone (L3)

Yield: 96%. M.p.: 245°C. FT-IR (KBr): υ, cm^{-1} 3241 (N–H), 3055 (H–N–C=S), 1638 (C=O), 1583 (C=N), 844 (C=S). UV–Vis (DMF): λ_{max}, nm (ε, $dm^3mol^{-1}cm^{-1}$) 322 (14,450) (n→π*transition), 246 (10,800) (π→π*transition). ^{1}H NMR (400 MHz, DMSO d_6): δ, ppm 11.51 (s, 1H, –N**H**–C=S), 9.08 (s, 1H, C**H**=N), 8.60 (t, *J* = 7.5 Hz, 1H, terminal N**H**), 8.16 (s, 1H, C2–**H**), 8.10-8.08 (dd, *J* = 10,2 Hz, 1H, C5–**H**), 7.80-7.84 (m, 1H, C6–**H**), 7.67-7.69 (d, *J* = 10 Hz, 1H, C8–**H**), 7.54-7.50 (m, 1H, C7–**H**), 2.51 (t, *J* = 4.5 Hz, 2H, –C**H**$_2$), 1.14 (t, *J* = 8.5 Hz, 3H, –C**H**$_3$). ^{13}C NMR (100 MHz, DMSO-d_6): δ, ppm 177.08 (C=S), 175.36 (C=O), 156.16 (C–O), 155.48 (C=N), 135.03, 134.22, 126.51, 125.61, 123.71, 119.15, 118.75 (aromatic carbons of chromone moiety), 38.73, 15 (ethyl carbons).

4-oxo-4H-chromene-3-carbaldehyde-4(*N*)-cyclohexylthiosemicarbazone (L4)

Yield: 92%. M.p.: 246°C. FT-IR (KBr): υ, cm^{-1} 3311(N–H), 3230 (H–N–C=S), 1636 (C=O), 1580 (C=N), 842 (C=S). UV–Vis (DMF): λ_{max}, nm (ε, $dm^3mol^{-1}cm^{-1}$): 322 (5,200) (n→π*), 242 (3,850) (π→π*). ^{1}H NMR (400 MHz, DMSO-d_6): δ, ppm 11.53 (s, 1H, –N**H**–C = S), 9.19 (s, 1H, C**H**=N), 8.19 (s, 1H, C2–**H**), 8.11 (d, *J* = 9.5 Hz, 2H, C5/C8–**H**), 7.84 (t, *J* = 10 Hz, 1H, terminal N**H**), 7.71 (d, *J* = 10.5 Hz, 1H, C6–**H**), 7.53 (t, *J* = 9.5 Hz, 1H, C7–**H**), 4.24-4.16 (m, 1H, cyclohexyl–**H**), 1.89-1.86 (d, *J* = 14 Hz, 2H, cyclohexyl–**H**), 1.76-1.73 (d, *J* = 15.5 Hz, 2H, cyclohexyl–**H**), 1.63-1.60 (d, *J* = 15 Hz, 1H, cyclohexyl–**H**), 1.44-1.10 (m, 5H, cyclohexyl–**H**). ^{13}C NMR (100 MHz, DMSO-d_6): δ, ppm 176.08 (C=S), 175.27 (C=O),

156.18 (C–O), 155.79 (C=N), 135.01, 134.52, 126.5, 125.64, 123.78, 119.18, 118.65 (aromatic carbons of chromone moiety), 53.18, 32.38, 25.64, 25.44 (cyclohexyl carbons).

4-oxo-4H-chromene-3-carbaldehyde-4(*N*)-phenylthiosemicarbazone (L5)

Yield: 98%. M.p.: 235°C. FT-IR (KBr): υ, cm^{-1} 3270 (N–H), 3207 (H–N–C=S), 1630 (C=O), 1562 (C=N), 843 (C=S). UV–Vis (DMF): λ_{max}, nm (ε, $dm^3mol^{-1}cm^{-1}$) 324 (17,500) (n→π*), 246 (12,850) (π→π*). ^{1}H NMR (400 MHz, DMSO-d_6): δ, ppm 11.95 (s, 1H, –N**H**–C=S), 10.15 (s, 1H, terminal N**H**), 9.31 (s, 1H, C**H**=N), 8.30 (s, 1H, C2–**H**), 8.12 (d, *J* = 10 Hz, 1H, C5–**H**), 7.84 (t, *J* = 10.5 Hz, 1H, C6–**H**), 7.71 (d, *J* = 10.5 Hz, 1H, C8–**H**), 7.56 (t, *J* = 7 Hz, 3H, C7–**H** and –C_6**H**$_5$), 7.39 (t, *J* = 9 Hz, 2H, –C_6**H**$_5$), 7.29 (t, *J* = 9 Hz, 1H, –C_6**H**$_5$). ^{13}C NMR (100 MHz, DMSO-d_6): δ, ppm 176.4 (C=S), 175.2 (C=O), 156.1 (C–O), 155.2 (C=N), 139.3, 135.2, 135.0, 128.6, 126.5, 125.9, 125.6, 123.7, 119.2, 118.5 (aromatic carbons of chromone and phenyl rings).

X-ray structure determination

X-ray diffraction data for complexes **1** and **3** were collected from a Bruker Quest X-ray (fixed-Chi geometry) diffractometer. The X-ray radiation employed was produced from a Mo-Iμs X-ray tube (K_α = 0.71073Å). The APEX3 software[1-4] was used to control the goniometer as well as for gathering the integrated intensity information for each reflection. The obtained data were corrected from absorption effects using the absorption correction program SADABS.[5] Absence of additional symmetry was confirmed using the program PLATON (ADDSYM).[6] Finally the structures were plotted, and the final data were refined using the software Olex2.[7]

Stability study of the Cu(II) complexes

The stability of complexes **1-5** was analysed by monitoring the electronic spectra of them in aqueous solution. The hydrolysis of these complexes in water, Tris-HCl and PBS buffer (with 1% DMSO) was monitored by UV-visible absorption spectra at a temperature of 27°C over a period of 72 h.

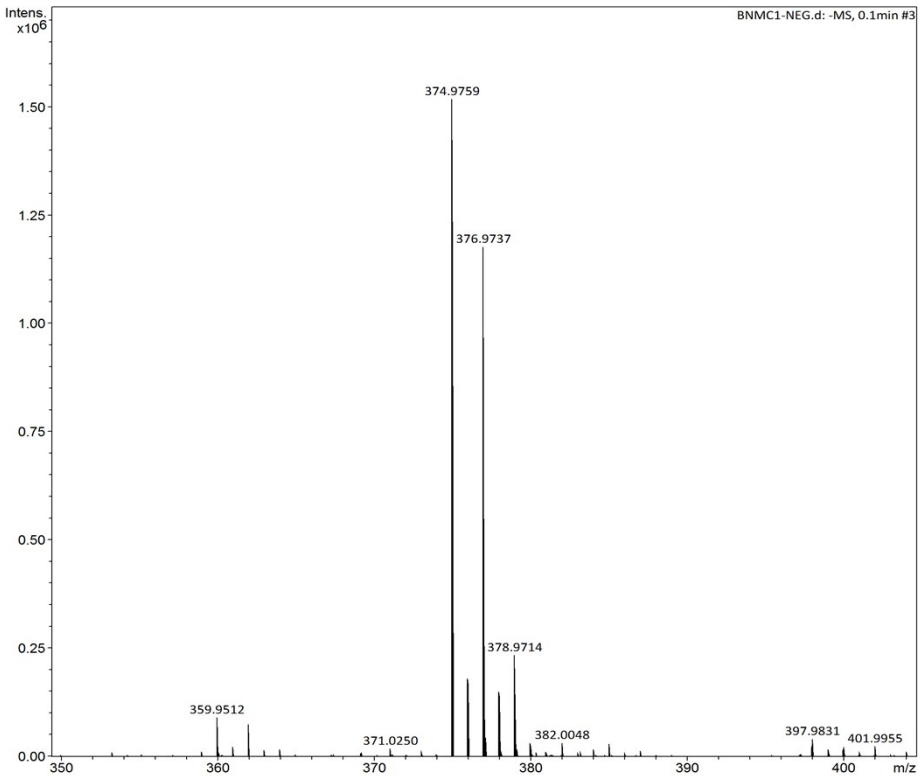

Fig. S1 ESI-MS spectrum of complex **1**.

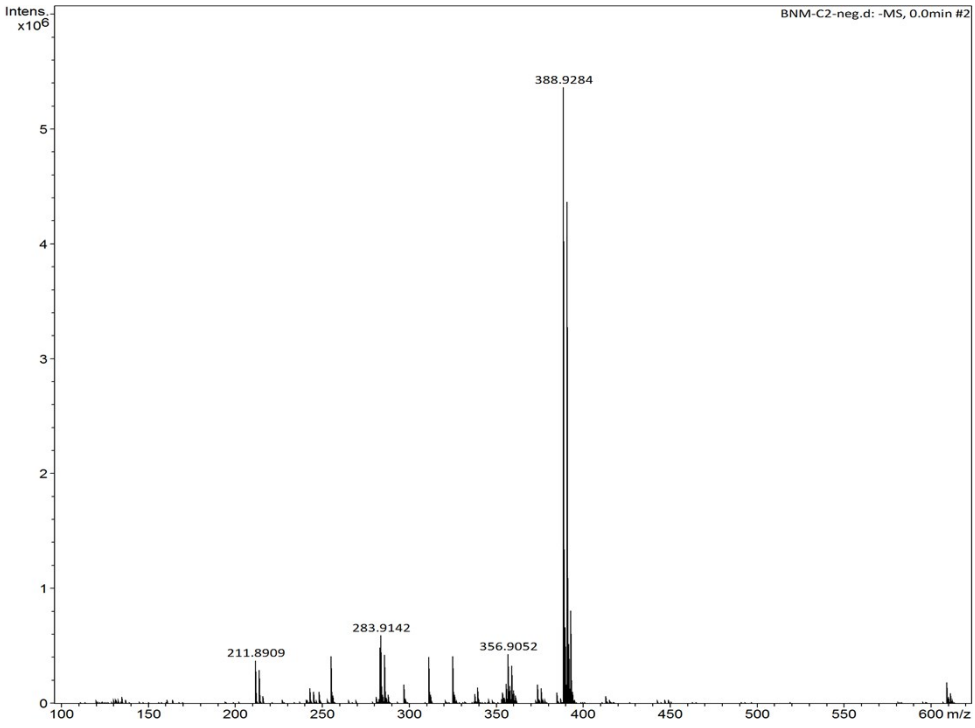

Fig. S2 ESI-MS spectrum of complex **2**.

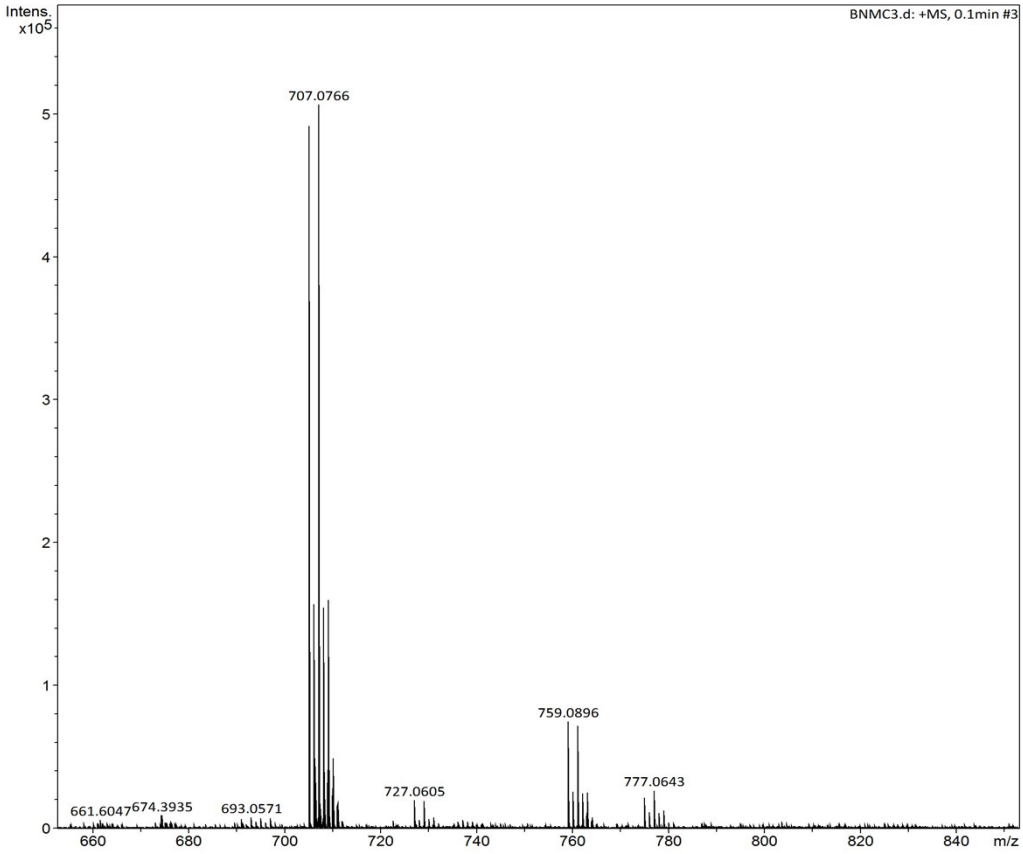

Fig. S3 ESI-MS spectrum of complex **3**.

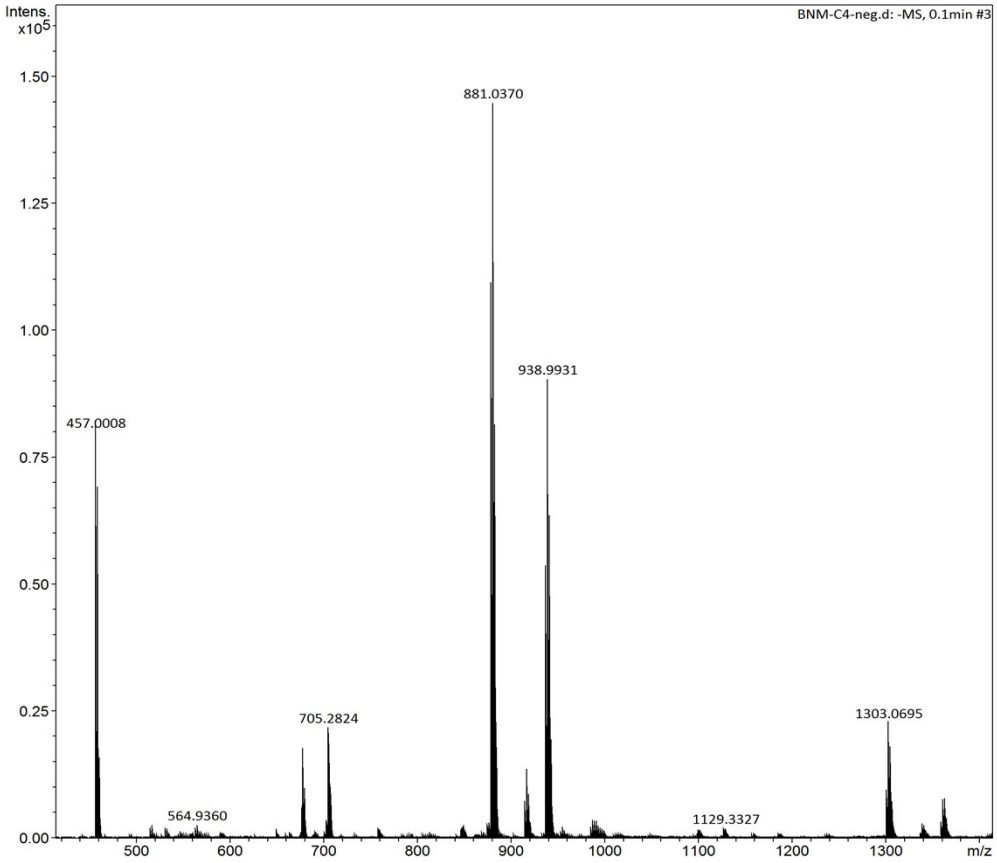

Fig. S4 ESI-MS spectrum of complex **4**.

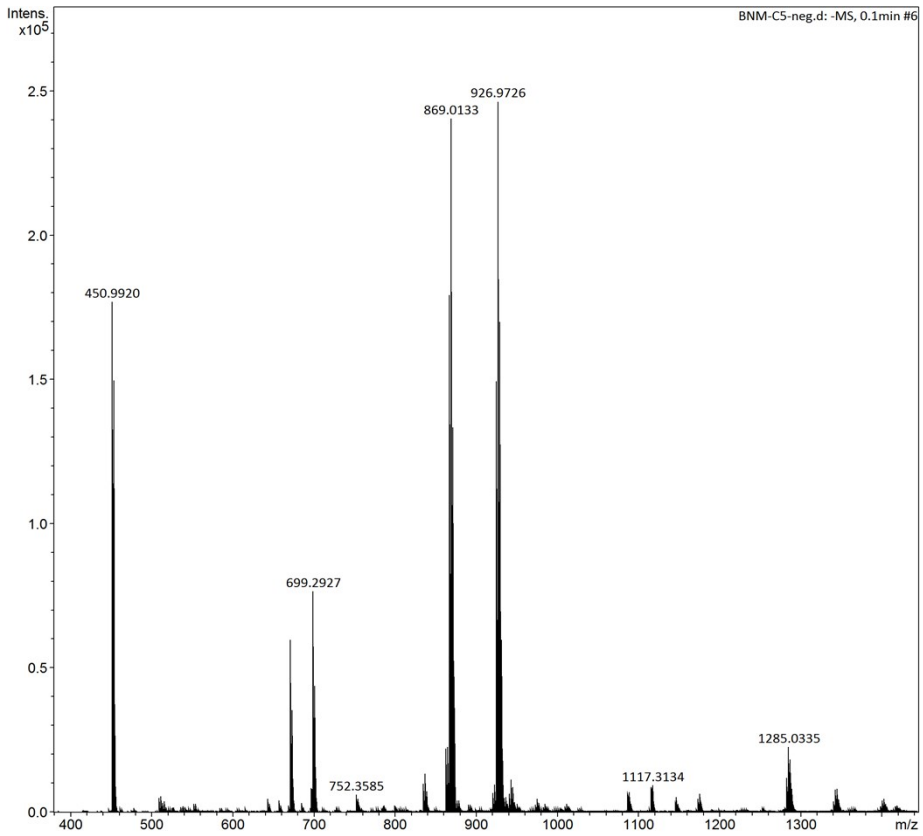

Fig. S5 ESI-MS spectrum of complex **5**.

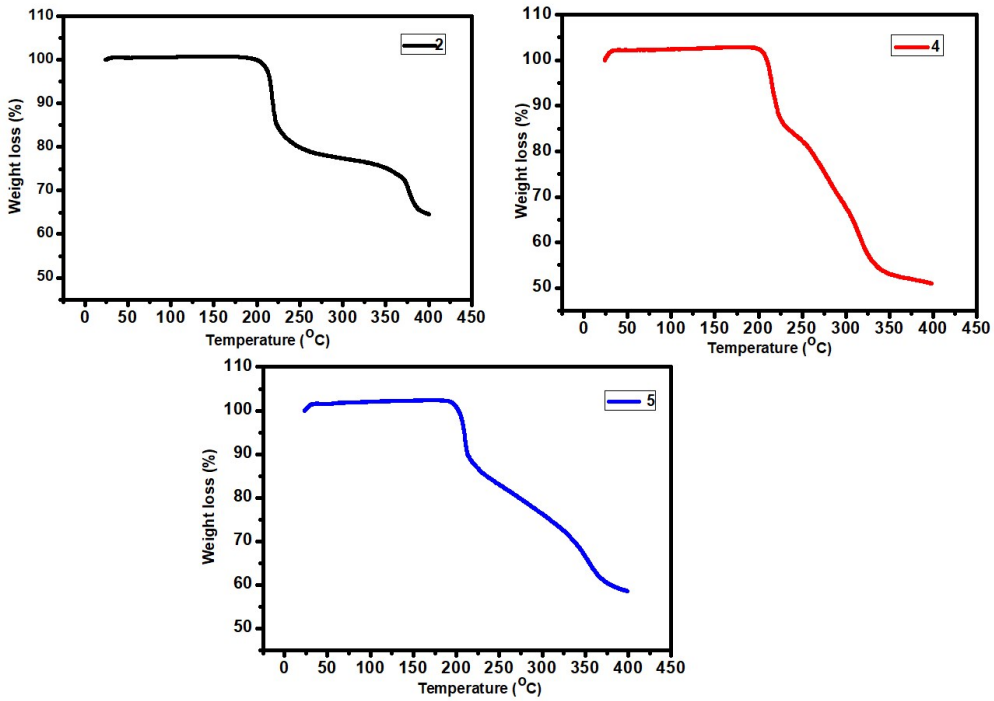

Fig. S6 Thermograms of complexes **2**, **4** and **5**.

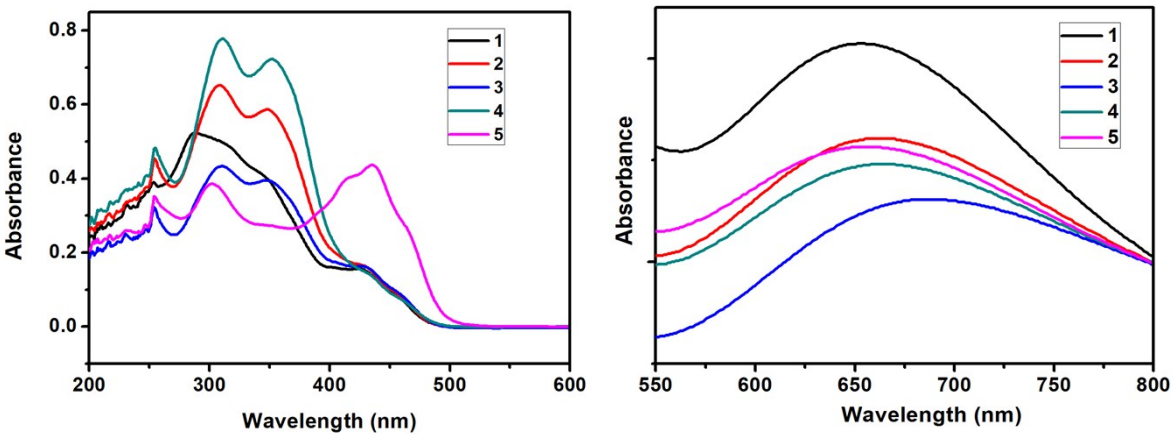

Fig. S7 UV-Visible spectra of complexes **1-5**.

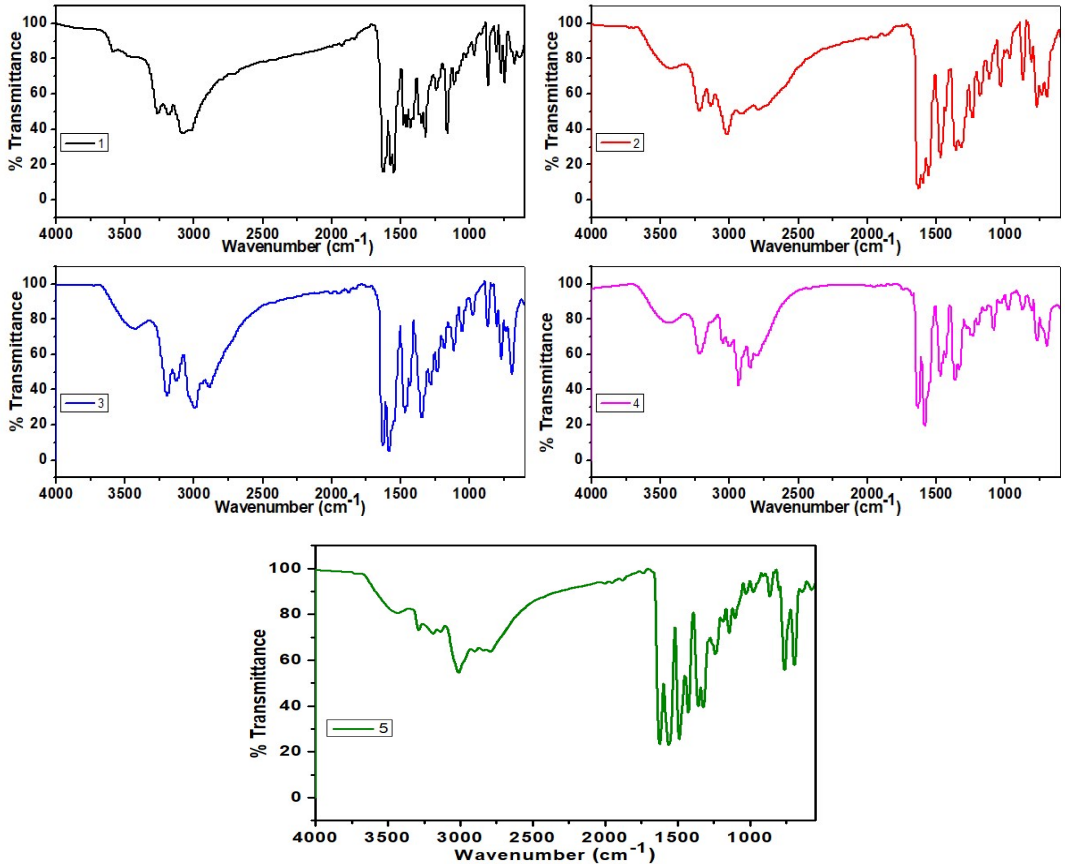

Fig. S8 FT-IR spectra of complexes **1-5**.

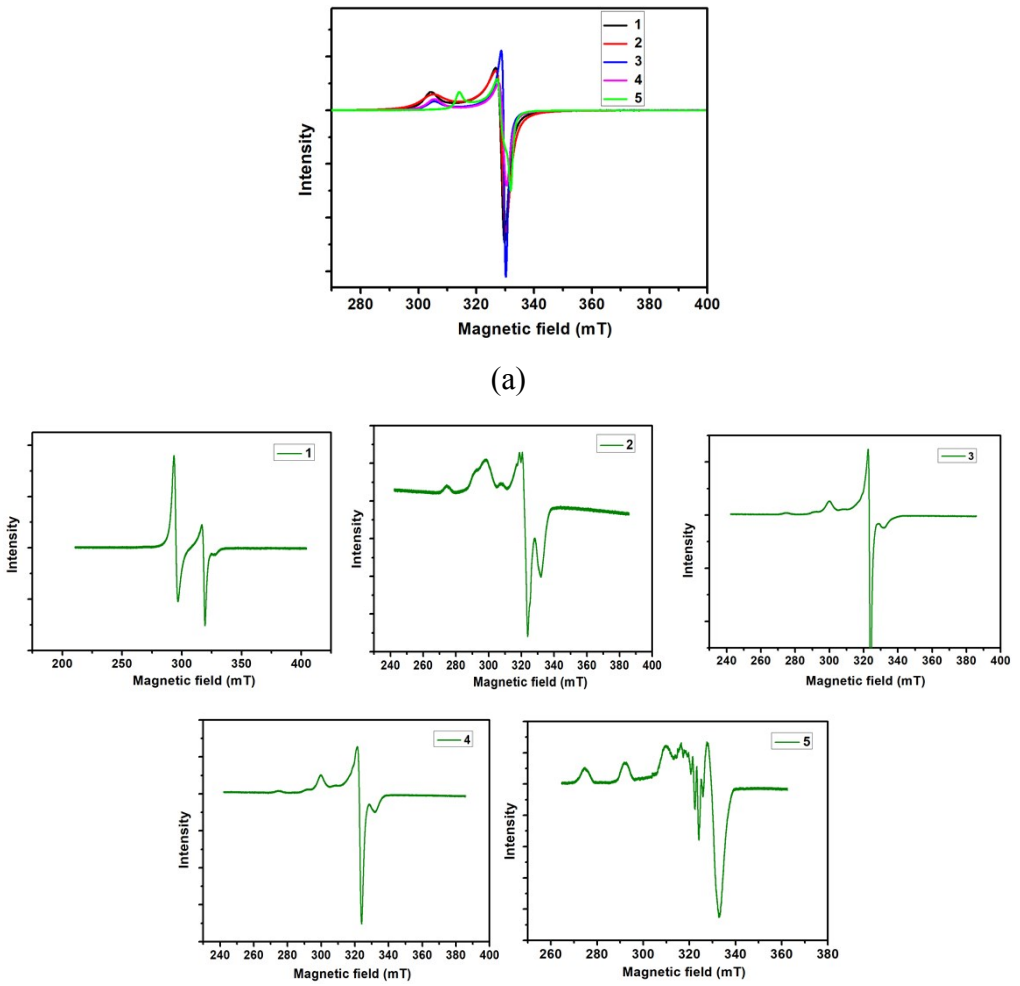

Fig. S9 EPR spectra of (a) the Cu(II) complexes in solid state at RT and (b) complexes **1-5** in frozen DMF at LNT.

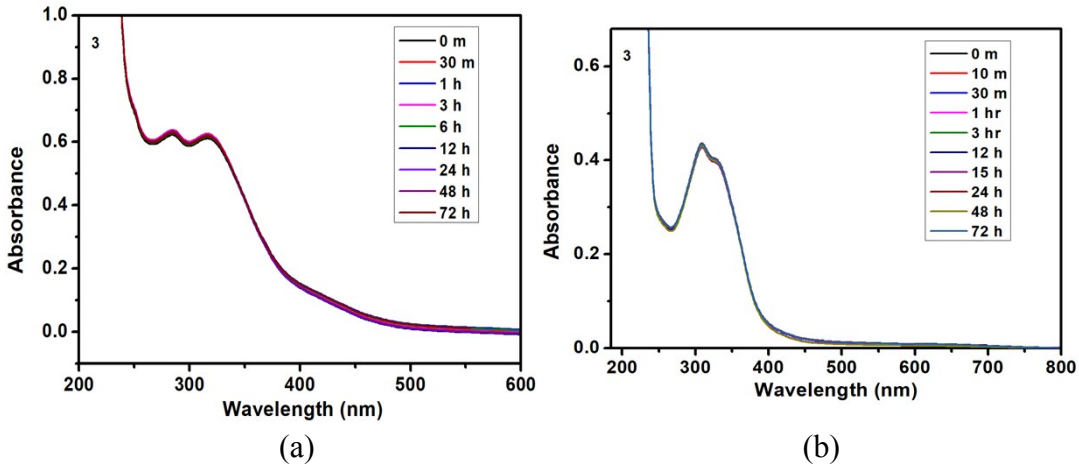

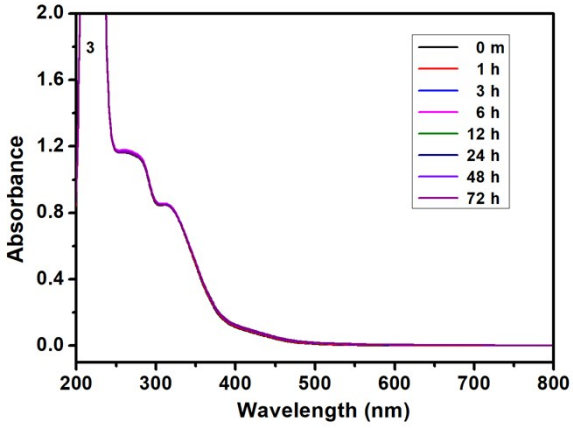

(c)

Fig. S10 Stability of complex **3** in (a) 1:99 DMSO-H_2O, (b) 1% DMSO/Tris HCl buffer (pH = 7.4) and (c) 1% DMSO/PBS buffer (pH = 7.2).

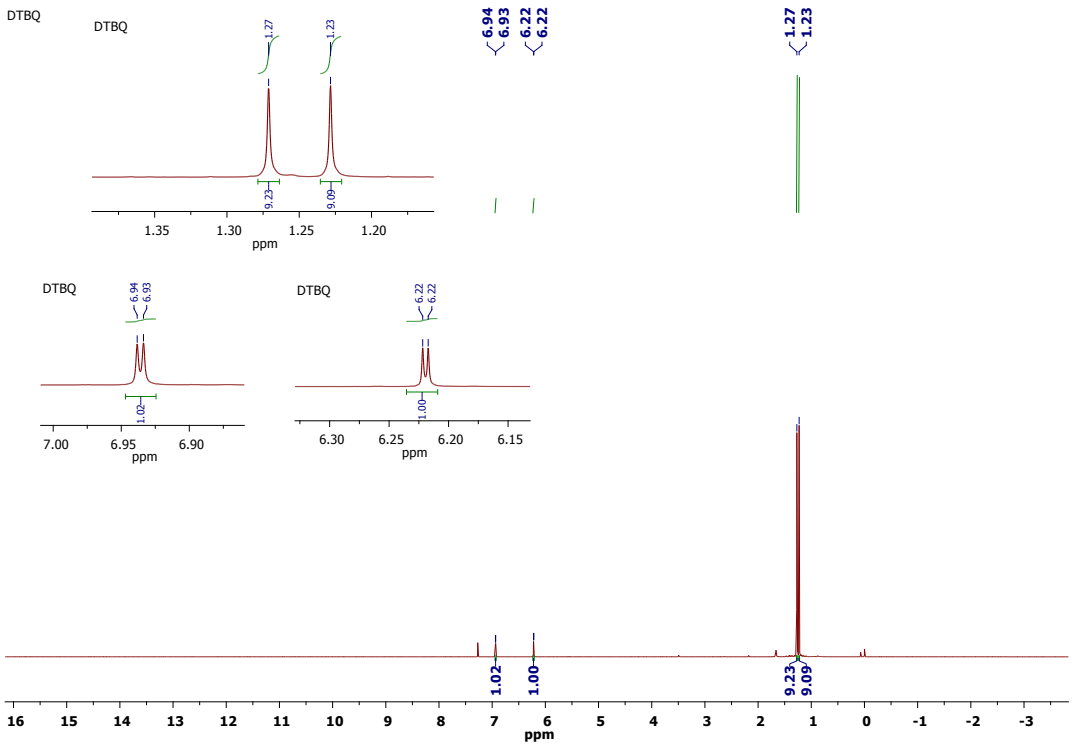

Fig. S11 ^{1}H NMR spectrum of isolated product 3,5-DTBQ.

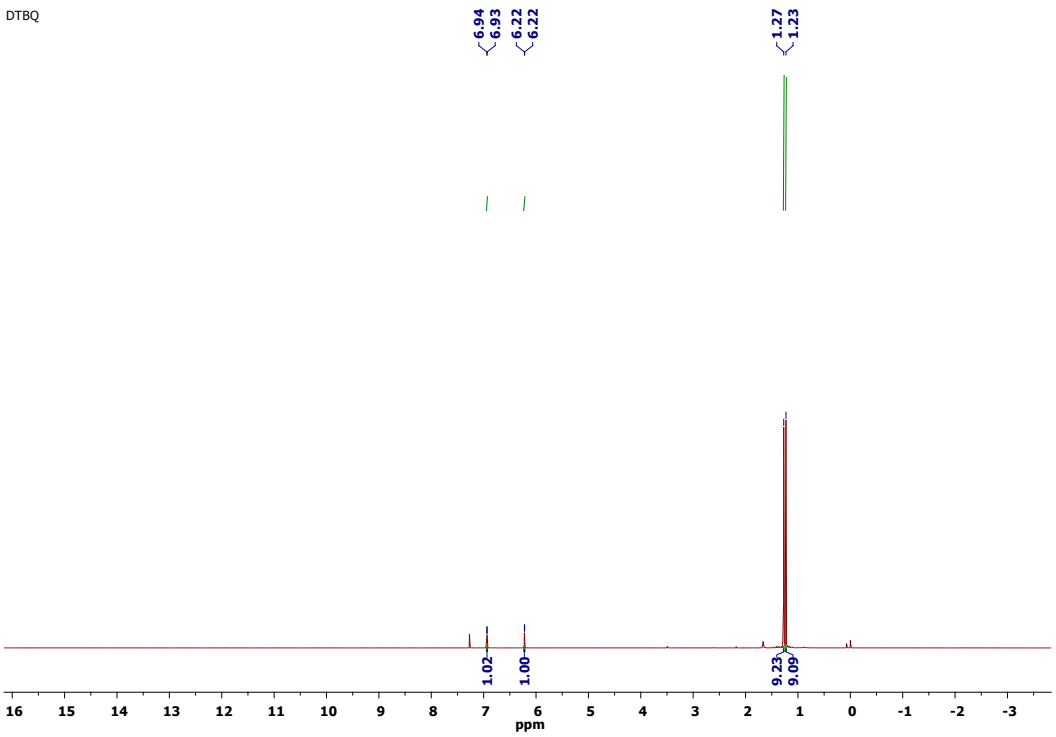

Fig. S12 ^{13}C NMR spectrum of isolated product 3,5-DTBQ.

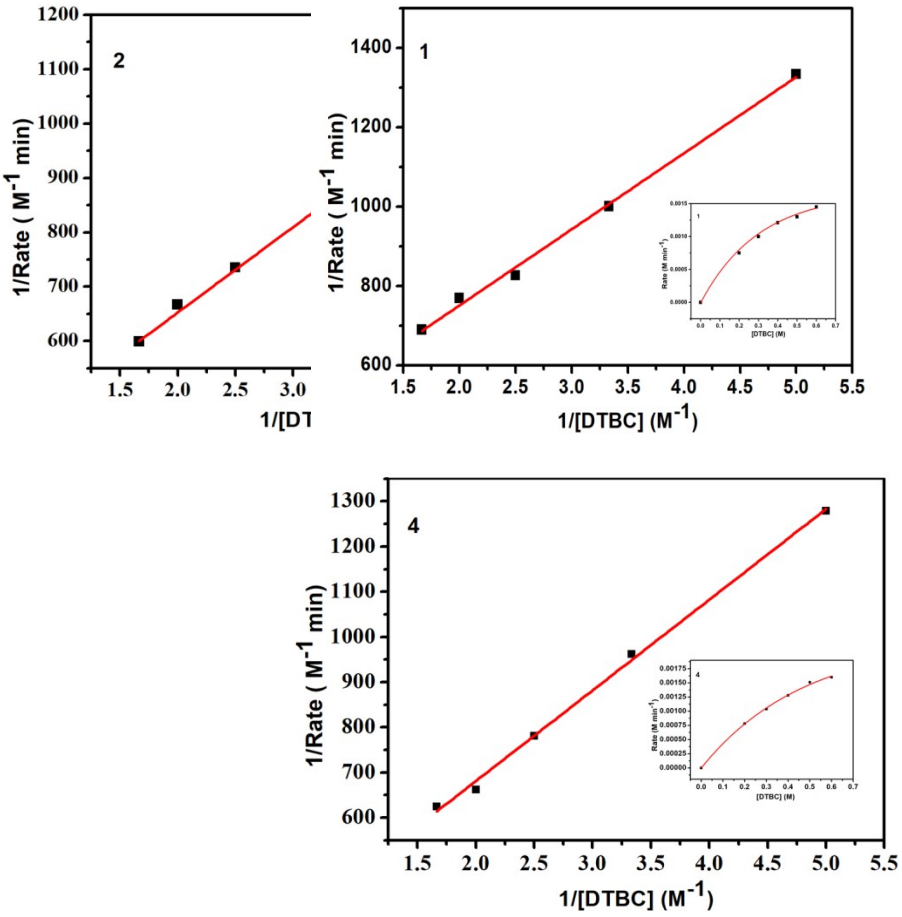

Fig. S13 Lineweaver-Burk plots for the oxidation of 3,5-DTBC catalysed by complexes **1**, **2** and **4** (Inset: Dependence of rate of catechol oxidation on 3,5-DTBC concentration).

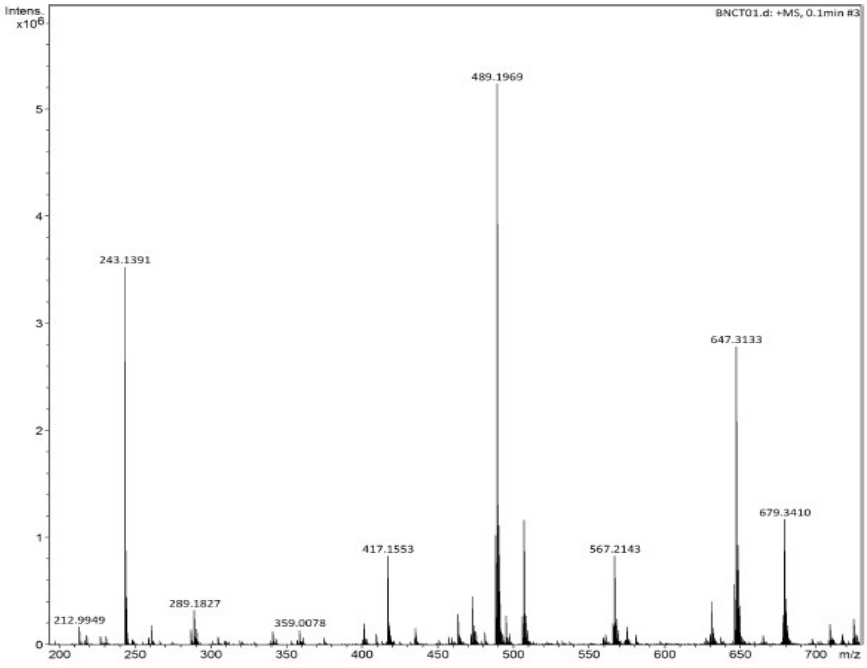

Fig. S14 ESI-MS spectrum of reaction (oxidation of 3,5-DTBC) mixture with catalyst **1**.

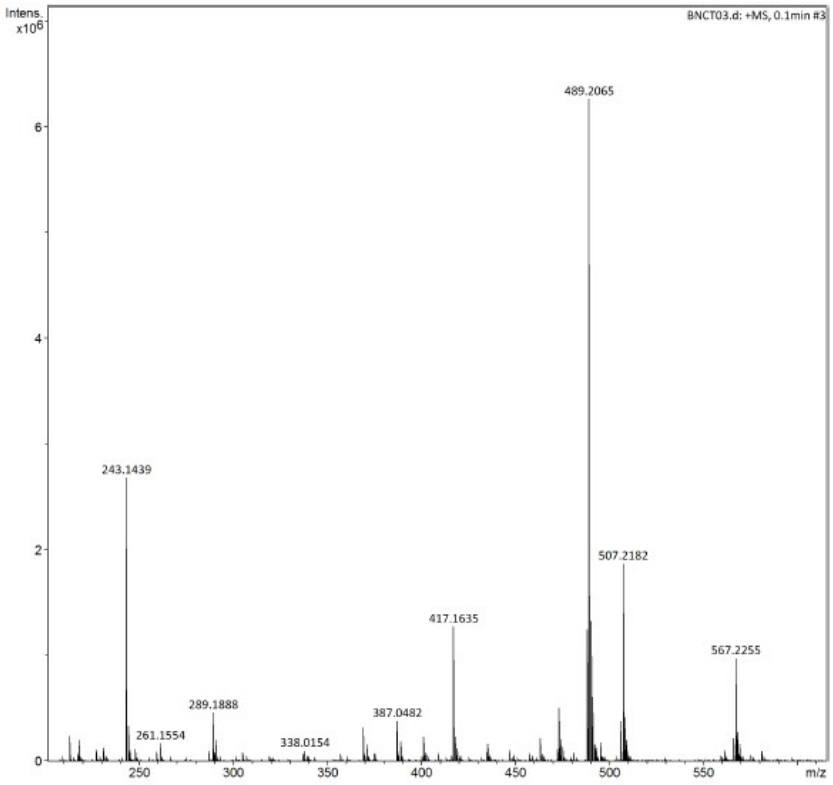

Fig. S15 ESI-MS spectrum of reaction (oxidation of 3,5-DTBC) mixture with catalyst **2**.

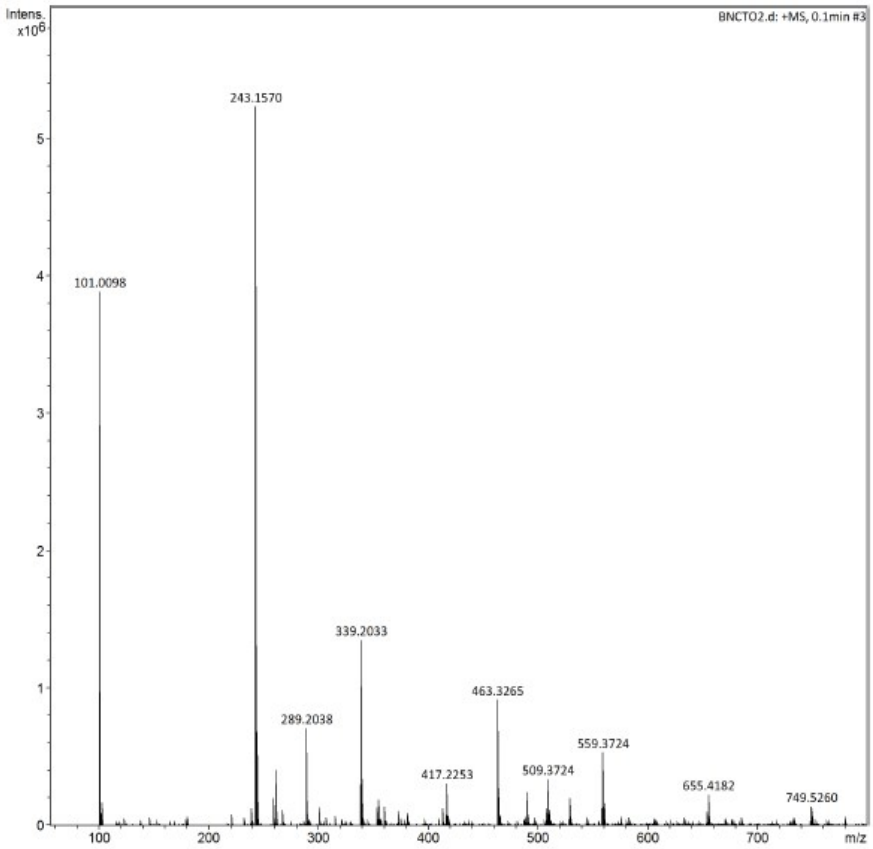

Fig. S16 ESI-MS spectrum of reaction (oxidation of 3,5-DTBC) mixture with catalyst **3**.

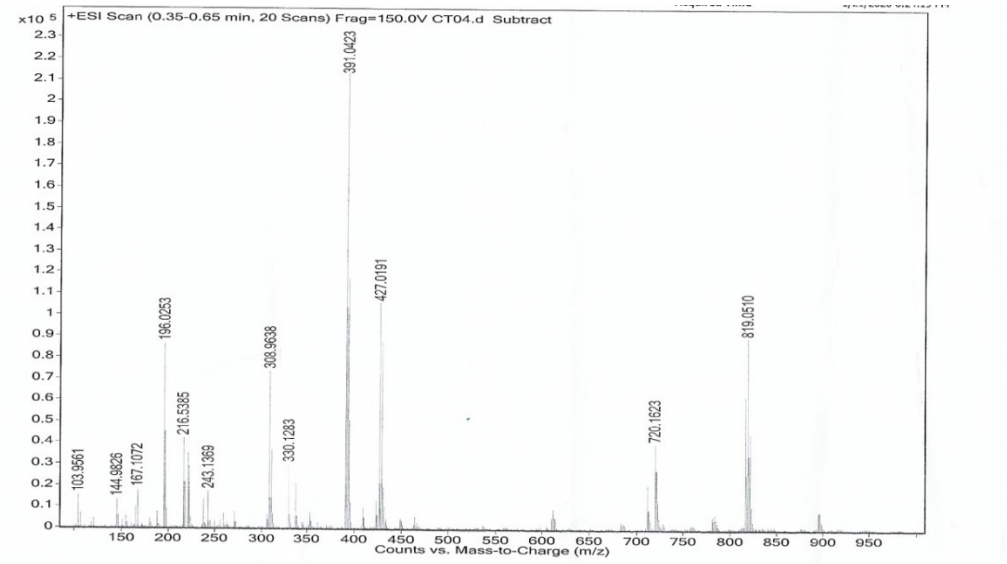
x10 5
+ESI Scan (0.35-0.65 min, 20 Scans) Frag=150.0V CT04.d Subtract
391.0423
427.0191
196.0253
819.0510
308.9638
216.5385
720.1623
330.1283
103.9561
144.9826
167.1072
243.1369
Counts vs. Mass-to-Charge (m/z)

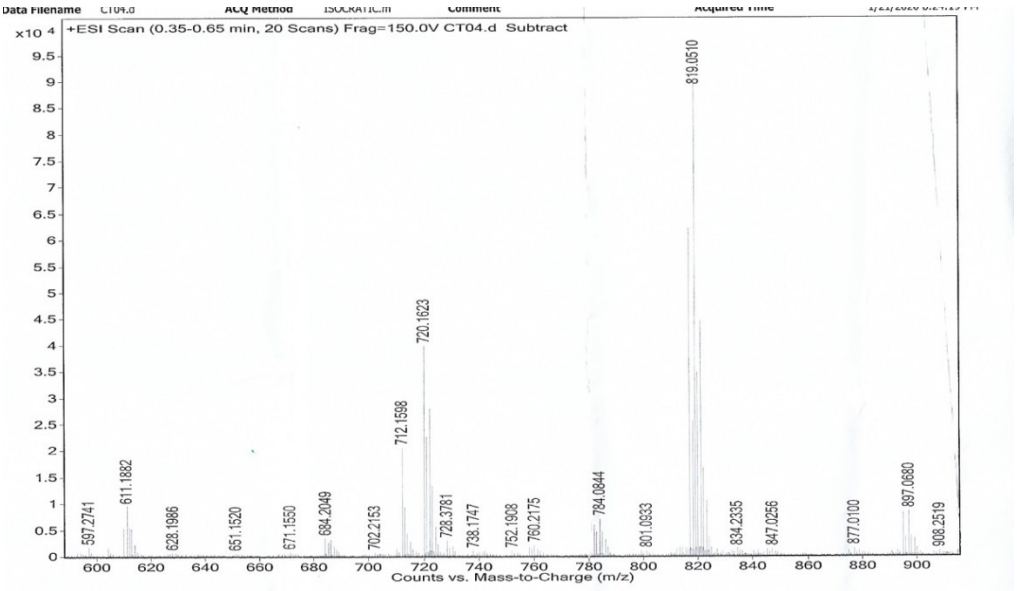

Fig. S17 ESI-MS spectrum of reaction (oxidation of 3,5-DTBC) mixture with catalyst **4**.

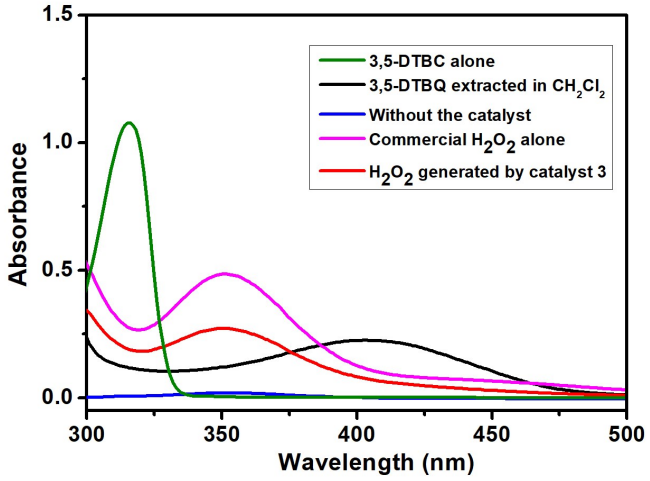

Fig. S18 Detection of H_2O_2 in the presence and absence of the catalyst.

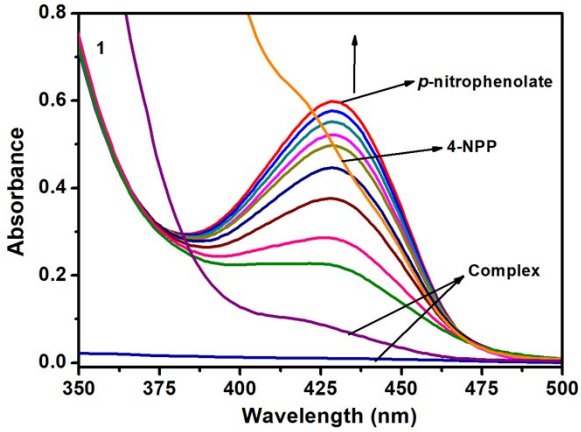

(a)

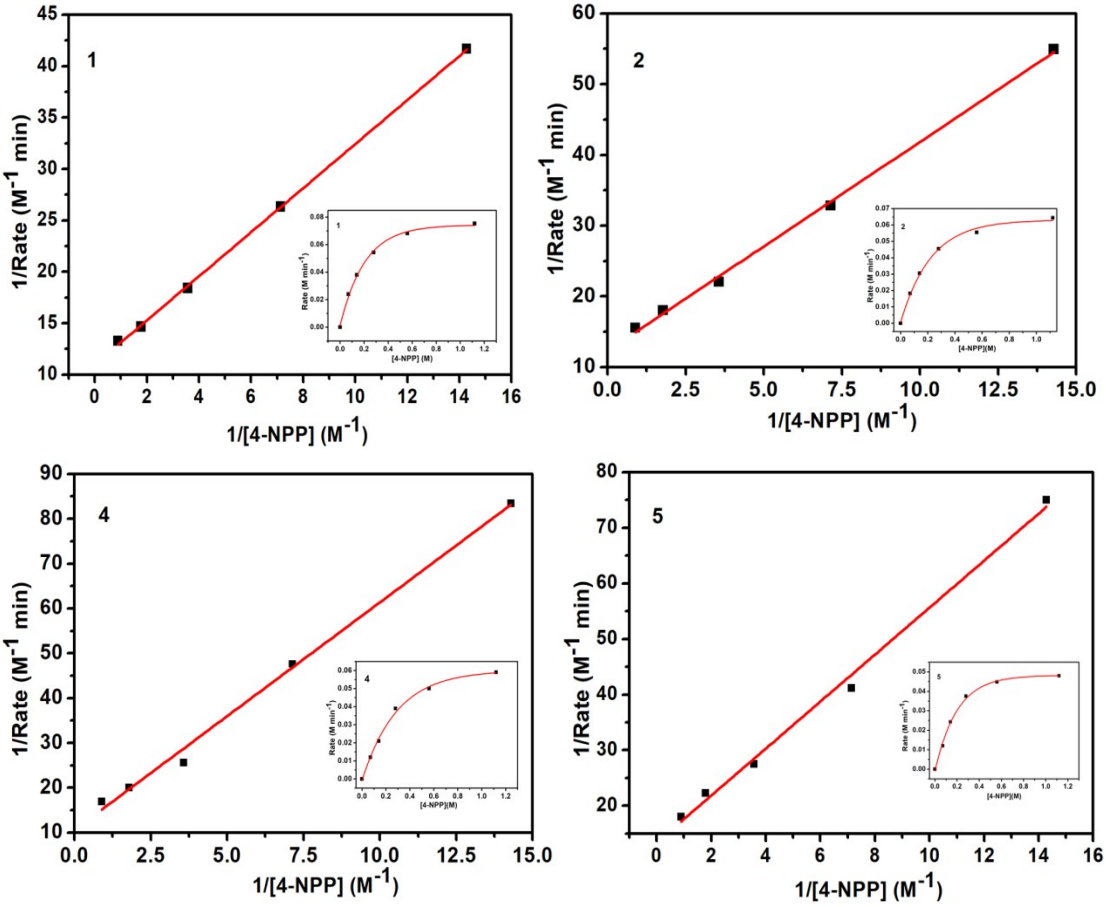

(b)

Fig. S19 (a) Hydrolysis of 4-NPP catalysed by complex **1 (**0.0138 M) to 20 equivalents of the substrate in DMF-water medium **as** observed by UV-Vis spectroscopy at 5 min time interval at 25°C and (b) Lineweaver-Burk plots for the hydrolysis of 4-NPP catalysed by complexes **1**, **2**, **4** and **5** (Inset: Dependence of rate of phosphatase-like activity on 4-NPP concentration).

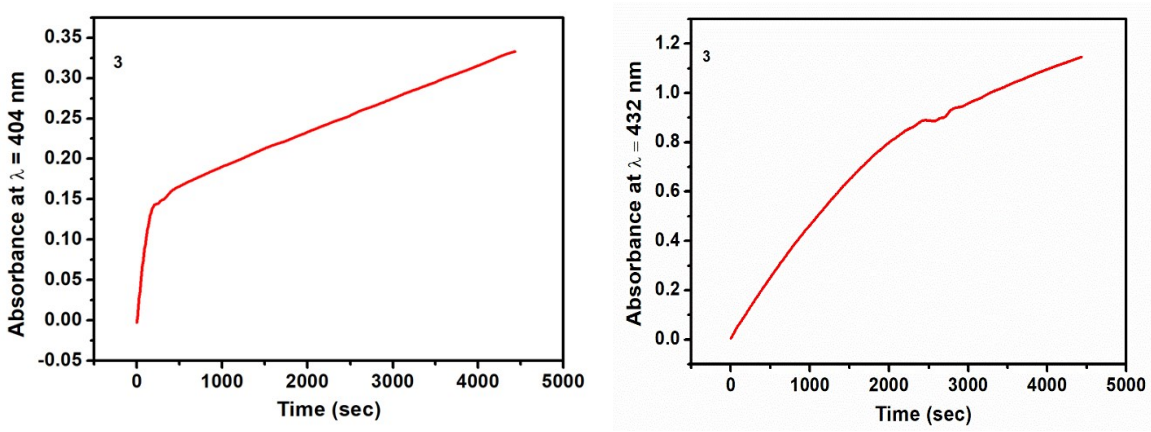

(a) (b)

Fig. S20 Absorption profiles due to (a) oxidation of 3,5-DTBC to 3,5-DTBQ (λ_{max} = 404 nm) catalysed by complex **3** and (b) the formation of *p*-nitrophenolate (λ_{max} = 432 nm) on addition of 4-NPP to complex **3**.

Binding of the complexes with biomolecules

DNA binding studies

Stock solutions of calf thymus (CT)-DNA were prepared in Tris-HCl buffer solution (pH = 7.4). The prepared CT-DNA solutions showed the UV-visible absorbance ratio of 1.85/1 at wavelengths 260/280 nm. This suggested the suitability of the prepared solution for various applications, since the above DNA purity test confirmed the absence of contaminants and proteins.[8] The DNA concentration per nucleotide was determined by absorbance spectroscopy using the molar absorption coefficient at 260 nm as 6600 $M^{-1}cm^{-1}$ with a dilution factor of 12.5.

The UV-Vis spectra of the test complexes (fixed concentration) with the gradual increase of DNA concentration were recorded. In order to find out the binding ability of the complexes, we employed the basic Wolfe-Shimmer equation[9]

$$[DNA]/(\varepsilon_a-\varepsilon_f) = [DNA]/(\varepsilon_b-\varepsilon_f) + 1/K_b\,(\varepsilon_b-\varepsilon_f) \qquad (S1)$$

The intrinsic binding constant (K_b) values of the analytes were determined from the ratio of the slope to the y-intercept in the plot of $[DNA]/(\varepsilon_a-\varepsilon_f)$ *vs* [DNA].

The varying amounts of the complexes were added incrementally to the fixed concentration of CT DNA bound with ethidium bromide (EB), and emission spectra were recorded during each addition. To quantitatively relate the binding propensity of the Cu(II) complexes, the apparent DNA binding constants (K_{app}) were determined using the equation[10]

$$K_{EB}\,[EB] = K_{app}\,[Complex]_{50} \qquad (S2)$$

where, $[Complex]_{50}$ is the concentration of complex at 50% reduction in the emission intensity of EB bound DNA, K_{EB} (1.0×10^7 M^{-1}) is the DNA binding constant of EB, and [EB] is EB concentration (5 μM). The quenching constants (K_{sv}) were obtained from the slopes of straight lines of the Stern-Volmer equation[11]

$$F_0/F = K_{SV}[Q] + 1 \qquad (S3)$$

where F_0 and F are the emission intensities in the absence and presence of quenchers respectively.

The viscosity values were measured in triplicates and the average viscosities were determined. Viscosity measurements of the CT-DNA (100 μM) solutions in the presence and absence of the complexes were carried out using a digital viscometer; temperature was maintained by an external thermostat at 25 ± 0.1°C. The relative viscosity $(\eta/\eta_0)^{1/3}$ values were plotted against the ratio of [Complex] to [DNA]. Here η represents the DNA viscosity in presence of the complex and η_0 represents the viscosity of DNA in buffer alone.[12]

BSA binding studies

The protein BSA (bovine serum albumin) was used for observing the interaction of the Cu(II) complexes. The proteins inherit the intrinsic fluorescence mainly due to the constituent amino acids namely tryptophan, tyrosine and phenylalanine.[13] To a fixed concentration of BSA (1 μM) prepared in PBS buffer (pH = 7.2), the complex (0-30 μM) was added incrementally, and its fluorescence intensities were noted. The fluorescence quenching spectra of the tryptophan residues at 346 nm ($\lambda_{excitation}$ = 280 nm) along with the synchronous fluorescence quenching spectra at two offsets ($\Delta\lambda$ = 60 and 15 nm) were recorded at room temperature. The excitation and emission slits were set at 2.5 and 1.25 nm respectively. The strengths of binding of the complexes with BSA were determined using Scatchard equation[14] (Eq. S4) and compared.

$$\log [(F_0 - F)/F] = \log K_{bin} + n \log [Q] \qquad (S4)$$

The values of equilibrium binding constant (K_{bin}) were found as antilogarithm of the intercept, and the number of binding sites (n) was calculated as slope of the plot, log $[(F_0 - F)/F]$ *vs* log [Q].

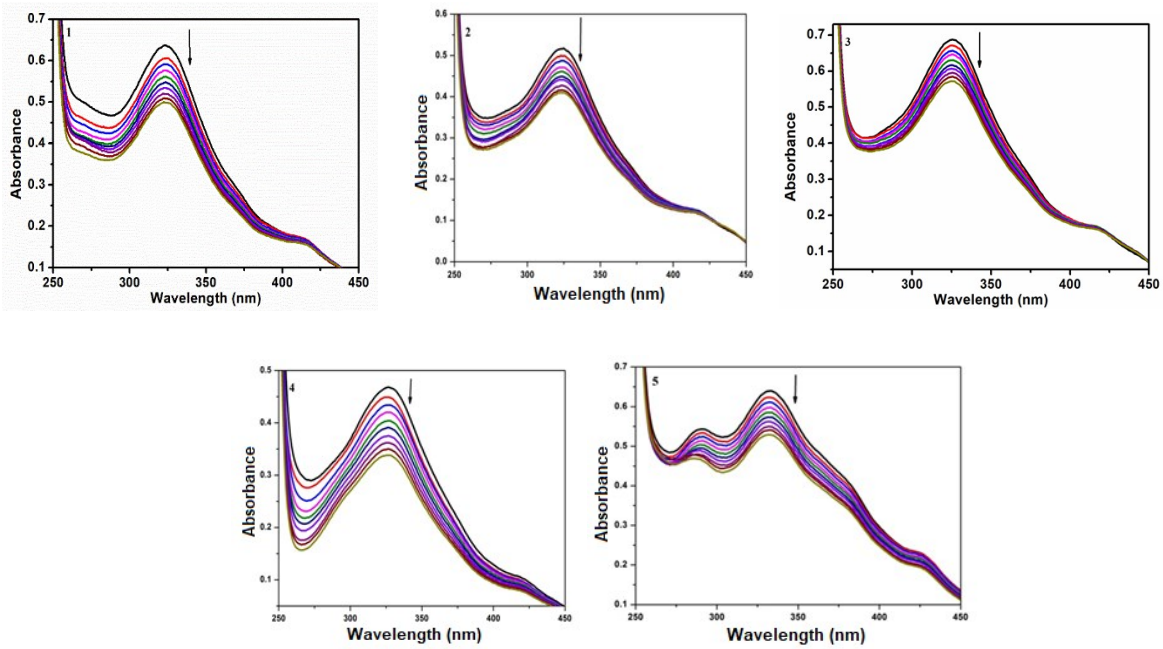

Fig. S21 Absorption spectra of complexes **1-5** in Tris-HCl buffer upon addition of CT-DNA. [Complex] = 20 μM, [DNA] = 0-50 μM. The arrow shows that the absorption intensity decreases upon increasing CT-DNA concentration.

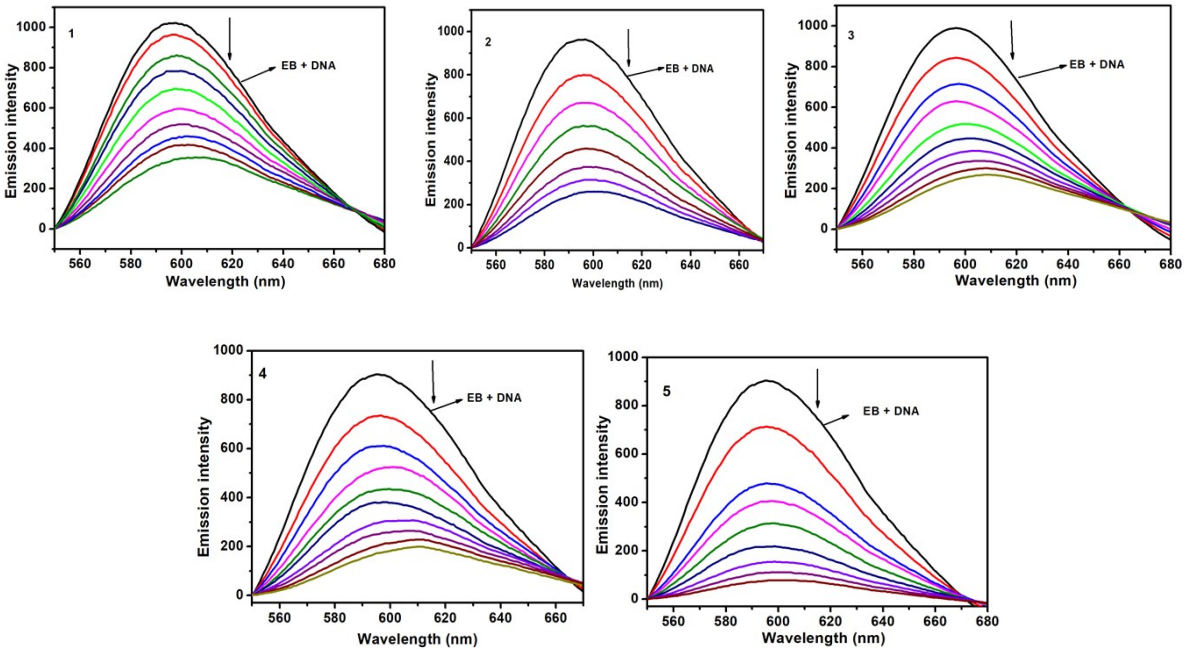

Fig. S22 Fluorescence quenching curves of EB bound DNA in the presence of complexes **1-5**. [DNA] = 5 μM, [EB] = 5 μM, [Complex] = 0−45 μM.

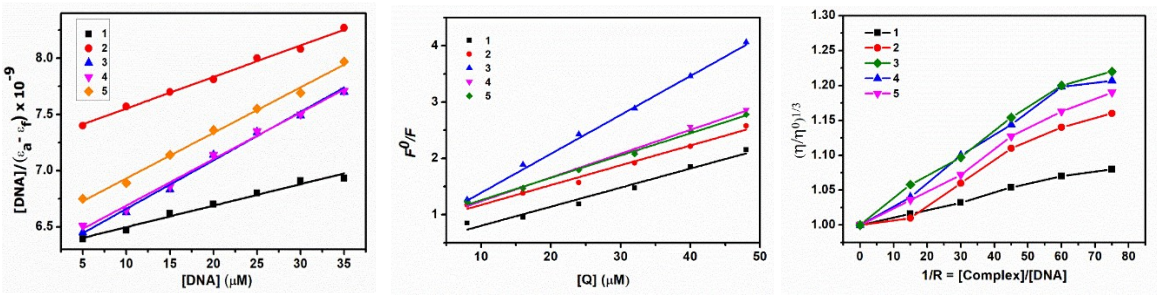

(a) (b) (c)

Fig. S23 (a) Plots of [DNA]/(ε_a−ε_f) *vs* [DNA] for the titration of the complexes with CT-DNA, (b) Stern-Volmer plots for fluorescence titrations of the complexes with CT-DNA and (c) Effect of the complexes on the viscosity of CT-DNA.

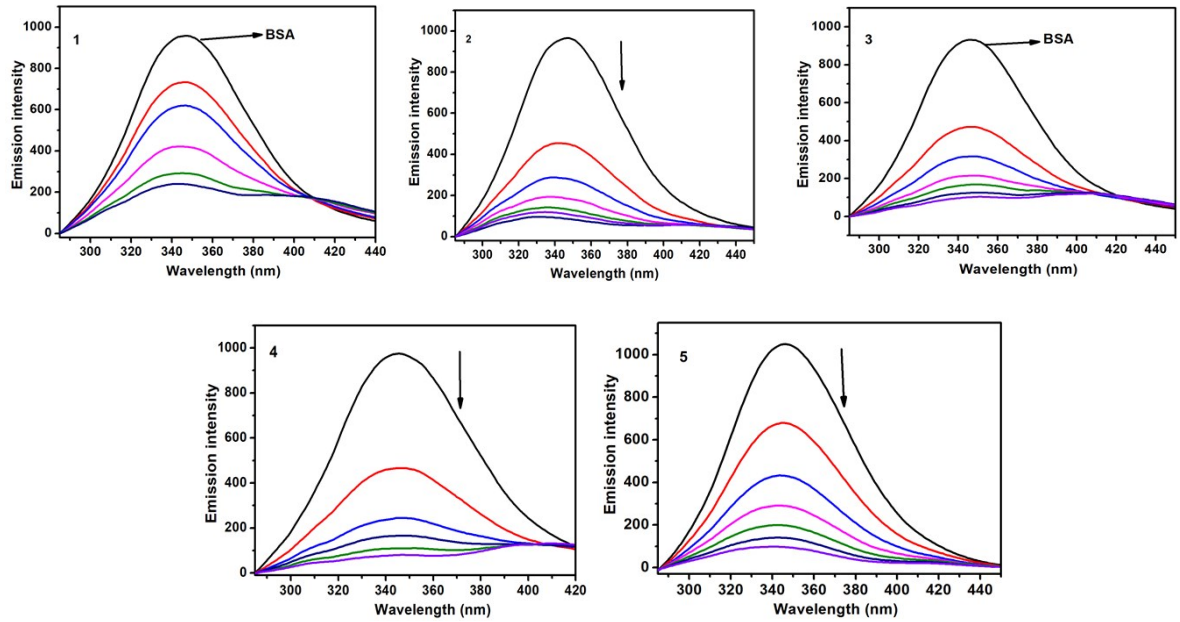

Fig. S24 Fluorescence quenching curves of BSA in the absence and presence of complexes **1-5**. [BSA] = 1 μM, [Complex] = 0-30 μM.

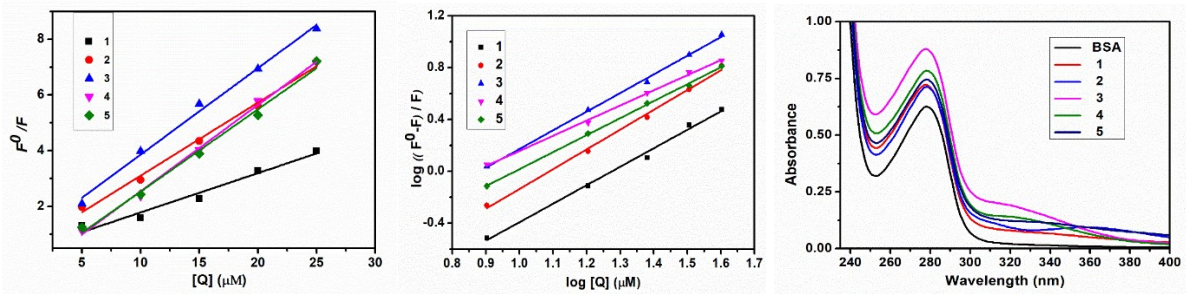

(a) (b) (c)

Fig. S25 (a) Stern-Volmer and (b) Scatchard plots of the fluorescence titrations of the complexes with BSA, and c) Absorption spectra of BSA (10 μM) in the absence and presence of the complexes (4 μM).

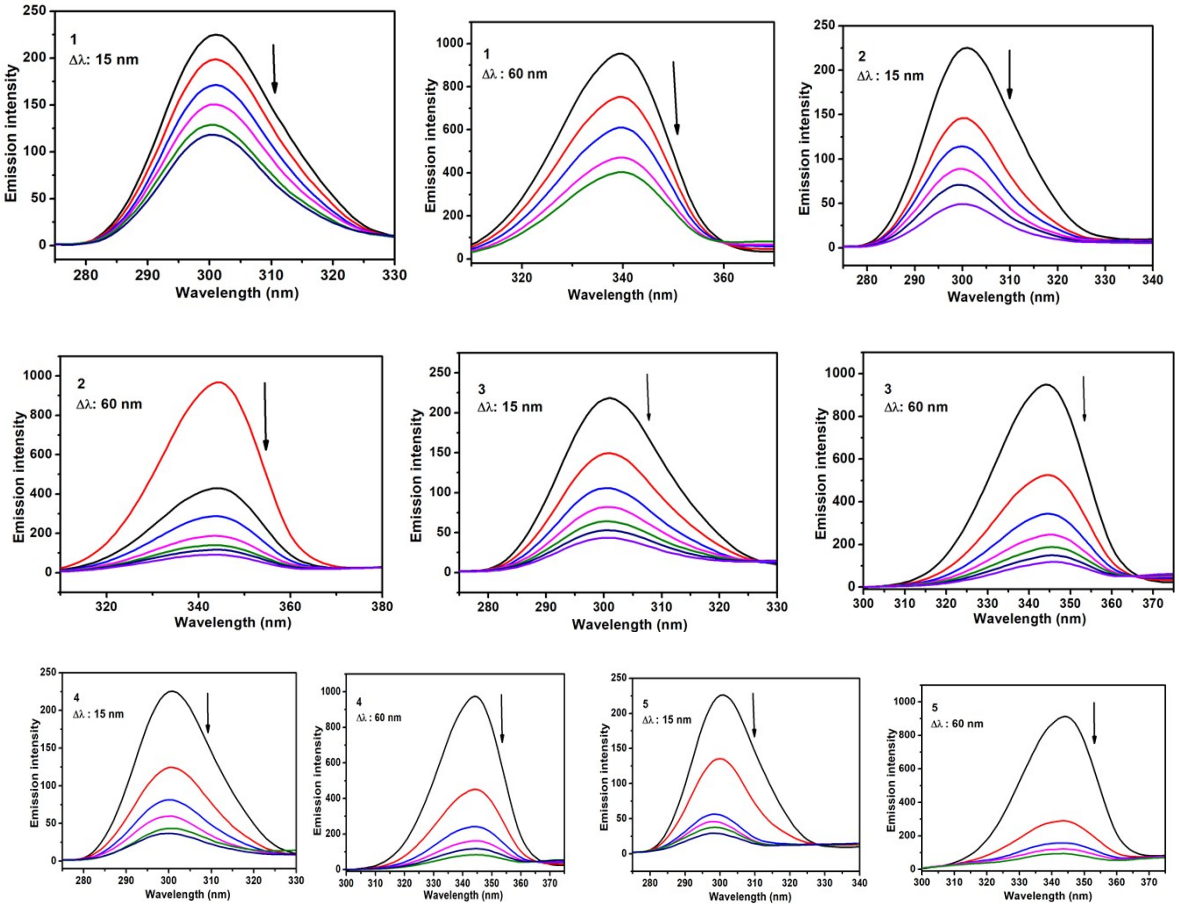

Fig. S26 Synchronous fluorescence spectra of BSA (1 μM) as a function of concentration of complexes **1-5** (0-30 μM) when Δλ = 15 or 60 nm.

Antioxidant studies

Antioxidants are substances which help in countering the adverse effects of excessive free radicals like reactive oxygen species present in the body by detoxifying them, thereby reducing the conceivable cellular damage.[15] Hence, antioxidants play a key role in counteracting the oxidative damages instigated to various biomolecules like DNA, lipids and proteins, which trigger cancer, aging, inflammation, cardiovascular and neurodegenerative diseases.[16] In order to examine the antioxidant potential of the Cu(II) complexes, two widely used spectrophotometric techniques, DPPH and ABTS assays, were chosen. The DPPH assay shows the free radical scavenging activity due to the conversion of stable DPPH free radical (red colour) to its reduced form which is in yellow colour. To a 2.96 mL of ethanolic DPPH (0.1 mM) solution, different concentrations (10-1000 μM) of the complexes prepared in 40 μL of ethanol were added. The decrease in the absorption of DPPH solution after the addition of the complexes was then measured at λ = 517 nm.[17] Similarly, the ABTS assay relies on the measurement of the suppression of absorbance at 734 nm due to the reduction of generated

green-blue coloured ABTS cation radical by antioxidants to a colourless solution.[18] Various concentrations of the complexes (1-100 μM) were added to 2.75 mL of ABTS solution. The percentages of the free radical scavenging activity (RSA) or inhibition activity of the complexes[19] were calculated using the following formula

$$\% \text{ RSA} = [(A_{control} - A_{sample})/(A_{control})] \times 100 \quad \text{(S5)}$$

$A_{control}$ is the absorbance of the control (3 mL DPPH / ABTS), and A_{sample} is the absorbance of the sample / standard. IC_{50} values were calculated using the least squares regression analysis. The average values were determined from the three independent experiments. Gallic acid and ascorbic acid (10 mg/mL DMSO) were used as references.

Anti-haemolytic activity

Human erythrocytes (RBCs) are said to be one of the ideal drug delivery systems in the human body due to their specific characteristics. Hence, it is necessary to test the toxicity caused by the complexes towards RBCs of a healthy person.[20] RBCs were isolated and diluted with 0.1 M phosphate buffer saline (PBS) (pH 7.2). The solutions (10-1000 μg/mL) of the Cu(II) complexes were prepared and added to 0.5 mL of RBC solution. As a negative control, 0.5 mL of H_2O_2 was treated with PBS solution, as it caused complete degradation of RBCs. The sample without the complex and H_2O_2 (buffer alone) acted as a positive control.[21] Each of the samples was kept for incubation at 37°C and centrifuged at 1000 rpm for 10 min. The absorbance values of the supernatant solutions were noted spectrophotometrically at 540 nm. All the experiments were done in triplicate and inhibitory activities were determined and expressed as % inhibition of haemolysis

$$\% \text{ inhibition of haemolysis} = [(A_{control} - A_{sample})/(A_{control})] \times 100 \quad \text{(S6)}$$

$A_{control}$ and A_{sample} are the absorbances of the positive control and sample / standard respectively. Triton was utilised as a reference.

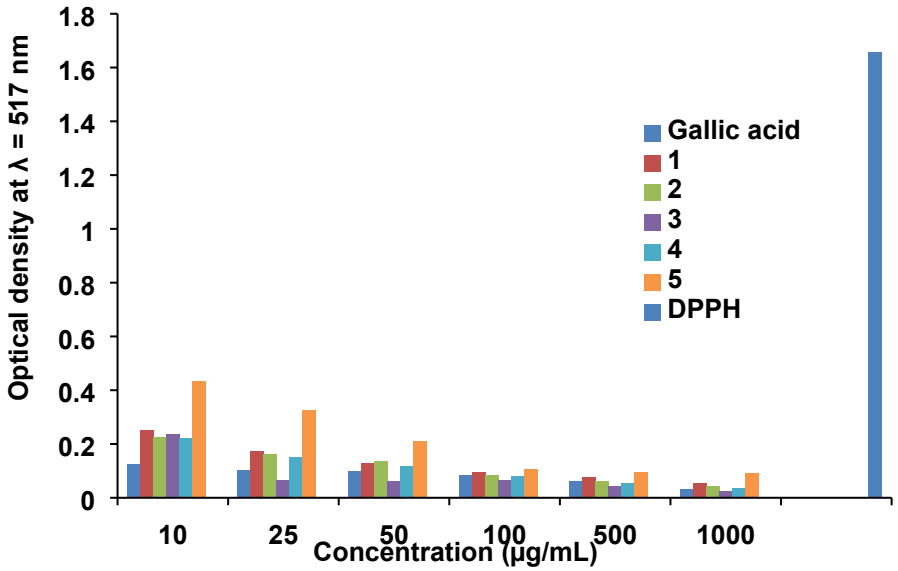

Fig. S27 DPPH assay of complexes **1-5** with reference to gallic acid.

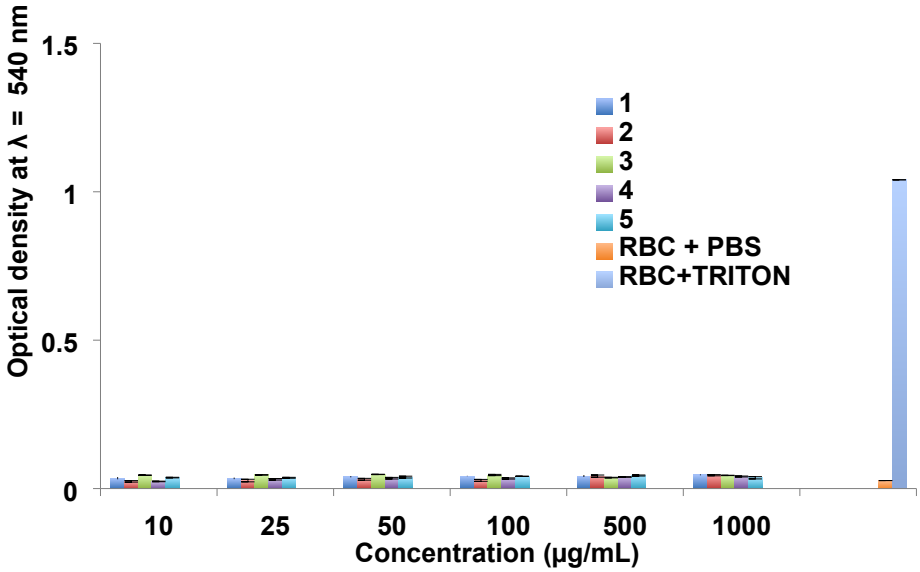

Fig. S28 Anti-haemolysis assay of complexes **1-5**.

Molecular docking with CASP3, VEGFR2 and PIM-1 kinase receptors

The target structures of CASP3, VEGFR2 and PIM-1 were retrieved from http://www.rcsb.org (PDB IDs are 1GFW, 1YWN and 1XWS respectively)[22], and processed by protein preparation wizard[23] where loops, bond orders and missing hydrogens were established. All the unnecessary heteroatoms along with water were removed, apart from the ones residing in the binding sites which were appropriately ionized at biological pH (7.4); later they were refined through optimization of hydrogen bonds. The receptor grid generation was done using the prepared protein by Glide software, version 6.6, Schrödinger, 2015.[24] Both the mononuclear (**1**) and binuclear (**3**) Cu(II) complexes were prepared by macro model

minimization with maximum iterations of 5000 using OPLS 2005 force field which is embedded in Prime.[25] In the case of the complexes, metal ions were defined based on their atom type and oxidation states. We employed molecular docking protocol called induced fit docking (IFD) with the purpose of keeping the receptor as flexible for docking studies. All the representations used for the ligand interaction analyses were employed *viz.* Pymol and Ligplot.[14]

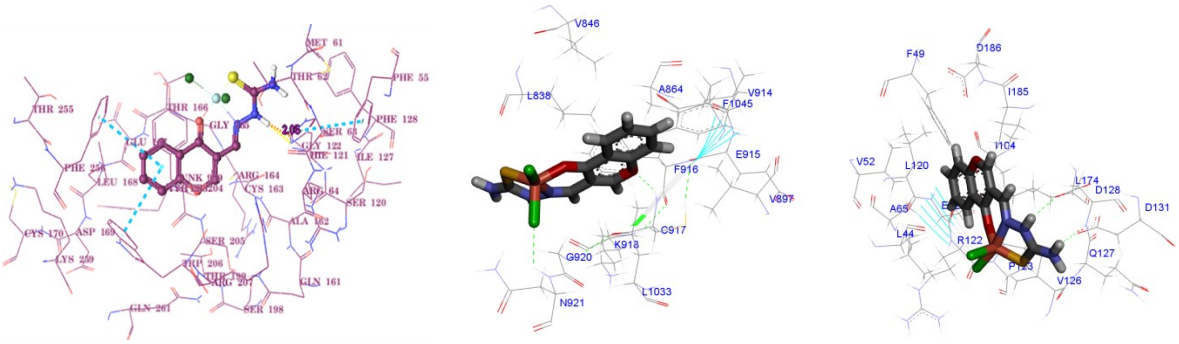

(a) (b) (c)

Fig. S29 Pymol view of the interactions of complex **1** with (a) CASP3, (b) VEGFR2 and (c) PIM-1 receptors.

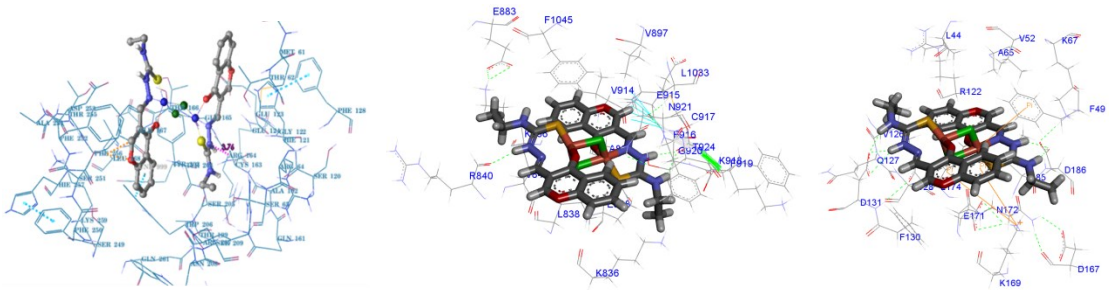

(a) (b) (c)

Fig. S30 Pymol view of the interactions of complex **3** with (a) CASP3, (b) VEGFR2 and (c) PIM-1 receptors.

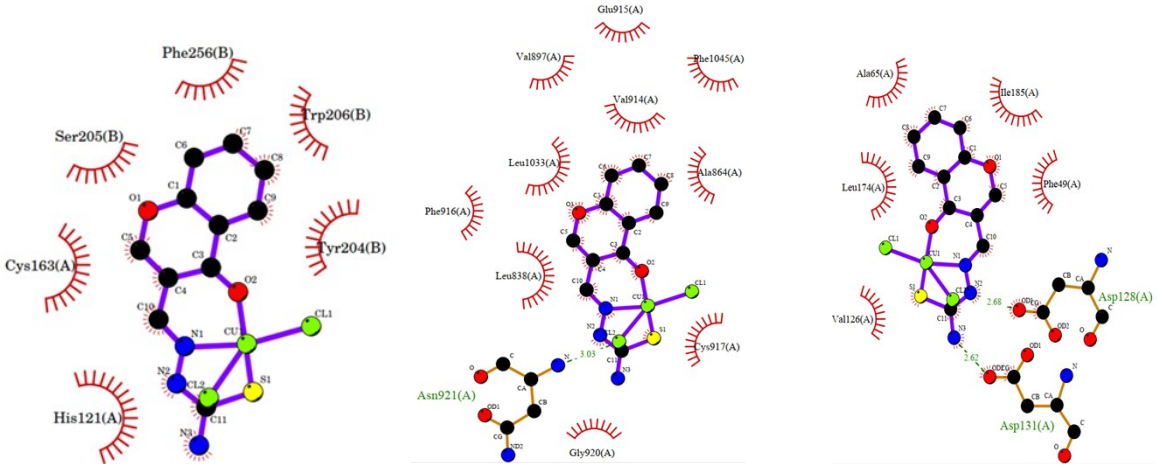

(a) (b) (c)

Fig. S31 Ligplot view of the interactions of complex **1** with (a) CASP3, (b) VEGFR2 and (c) PIM-1 kinase receptors.

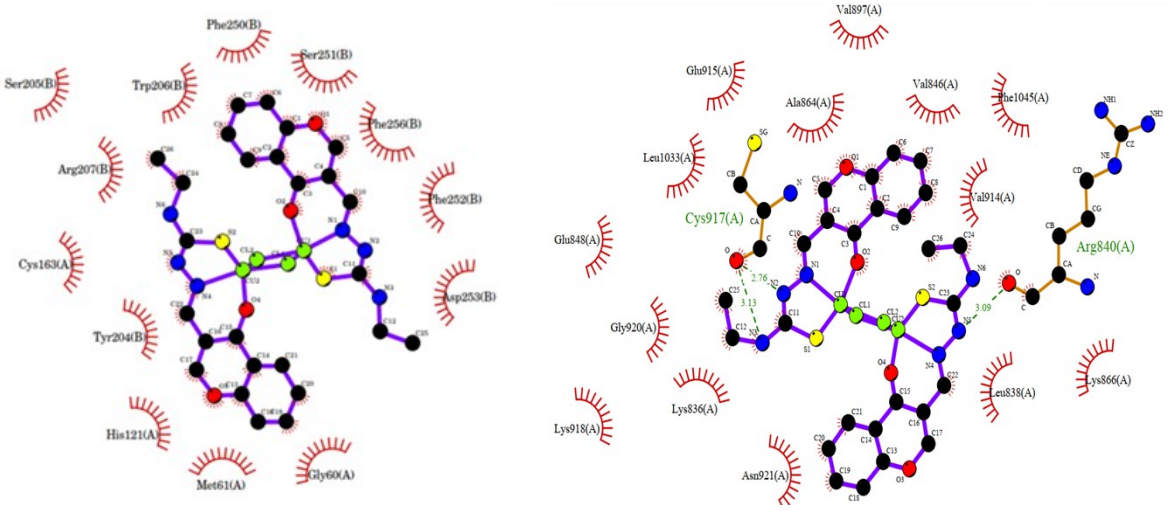

(a) (b)

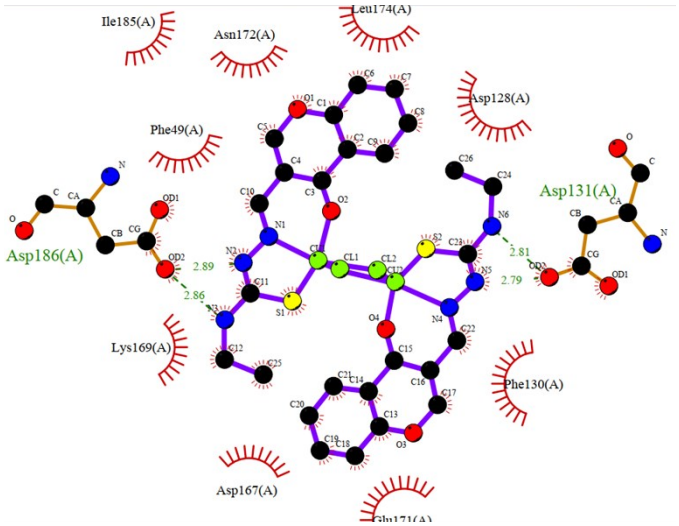

(c)

Fig. S32 Ligplot view of the interactions of complex **3** with (a) CASP3, (b) VEGFR2 and (c) PIM-1 kinase receptors.

***In vitro* cytotoxicity**

The *in vitro* cytotoxicity of the Cu(II) complexes was evaluated against human cervical cancer (Hela) cells (RCB0007, Tsukuba, Japan). The cells were maintained in standard Dulbecco's modified Eagle's medium (DMEM) supplemented with 10% fetal bovine serum (FBS) at 37°C under a humidified atmosphere of 5% CO_2 and 95% air. For the cytotoxicity evaluation, exponentially growing cells were harvested, plated in 96-well plates (2×10^3 cells/well) in DMEM and kept inside humidified 5% CO_2 incubator at 37°C for 24 h. After the cells had been washed with PBS, the medium was changed to serially diluted test samples in DMEM, with the control and blank in each plate. The cells were allowed to proliferate for 72 h, then washed twice with PBS, and a solution of 100 µL of DMEM containing 10% WST-8 (water soluble tetrazolium salts) available as cell counting kit (CCK-8) was added to each well. After incubating for 3 h, the absorbance at 450 nm was measured (Perkin Elmer EnSpire multilabel reader). Cell viability was calculated from the mean values of three wells using the following equation

$$Cell\ viability\ (\%) = \frac{(Absorbance\ of\ test\ sample\ -\ Absorbance\ of\ blank)}{(Absorbance\ of\ control\ -\ Absorbance\ of\ blank)} \times 100\% \quad \text{(S7)}$$

Colony formation assay

HeLa cells were seeded at a density of 5×10^3 cells/well in DMEM (1 mL/well) in a 12-well plate dish and incubated at 37°C in a CO_2 incubator for 12 h for the cell attachment. The medium was then changed to DMEM containing complex **3** at 0 (control), 2.5, 5 and 10 µM, and allowed the HeLa cells to get exposed for 24 h. Three replicates were made for each group. The cells were then washed twice with PBS, and the medium was replaced by fresh DMEM (2 mL) without any test compound. The cells were then allowed to grow for 10 days. On the last day, the cells were washed with PBS, fixed with 4% formaldehyde, and stained with crystal violet for 10 min. Finally, the colony area was measured[26] using ImageJ plugin, and the data were analysed by GraphPad software Prism 6.

Fluorescent microscopy and morphological studies

HeLa cells were seeded at a density of 2×10^5 cells/well in DMEM in a 60 mm dish and incubated for 24 h in a humidified CO_2 incubator to allow cell attachment. The cells were then washed twice with PBS, followed by treatment with complex **3** (10 µM) in DMEM, or in the case of the control cells, just DMEM. Both the treated and control cells were then incubated for 24 h, and then treated with AO/EB reagent. The cell morphology was captured

using Evos FL digital microscope (20× objective) with phase-contrast and fluorescence modes.[27]

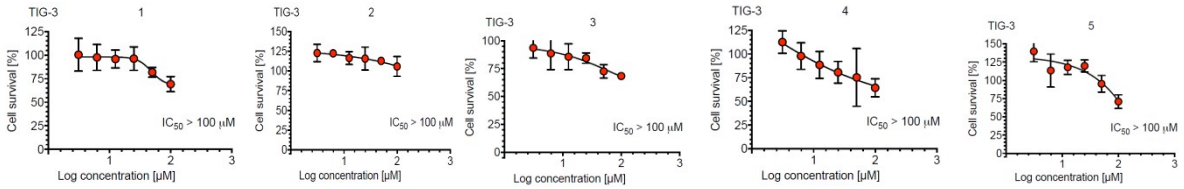

Fig. S33 Effect of the Cu(II) complexes against TIG-3 cells after 72 h of incubation.

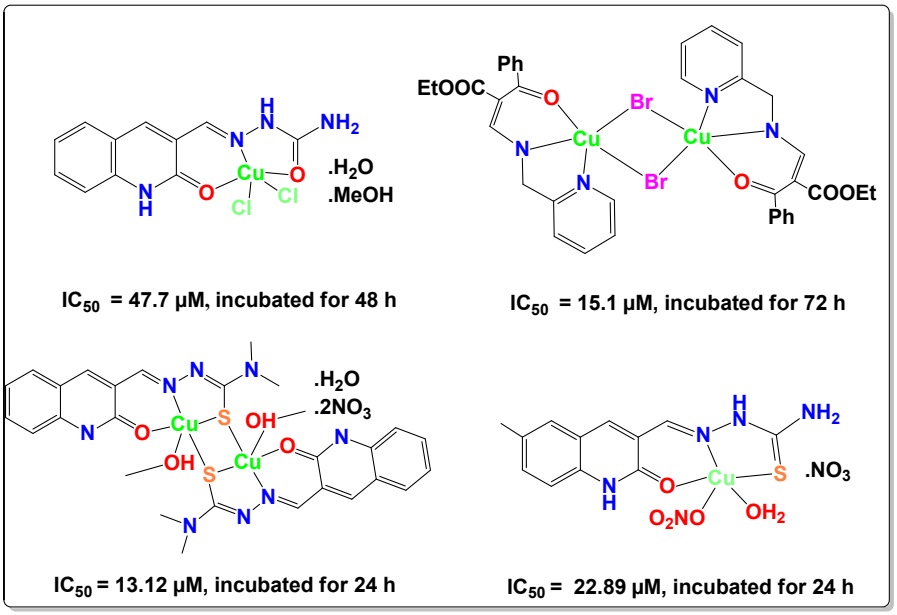

Fig. S34 Cytotoxicity of the reported Cu(II) complexes containing tridentate ligand(s) against HeLa cells.

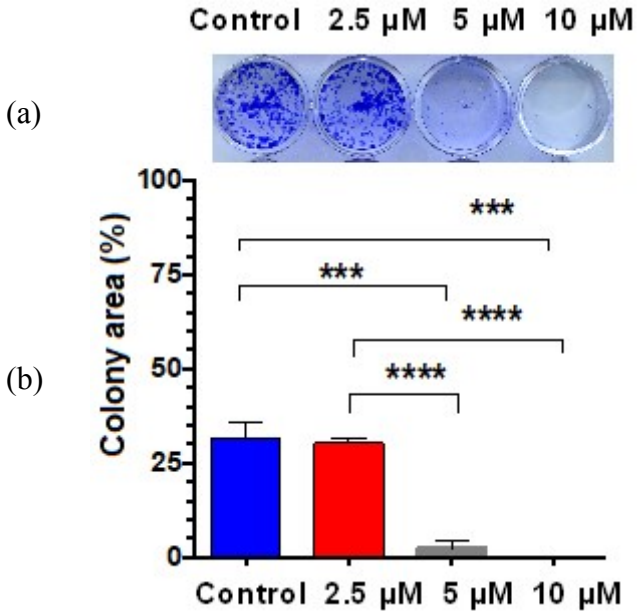

Fig. S35 Effect of complex **4** against colony formation of HeLa cells. (a) HeLa cell colonies treated with different concentrations of **4** and (b) Graph showing mean values of the area occupied by HeLa cell colonies (three replications), ***p < 0.001 and ****p < 0.0001 when compared with the untreated control, and among the treated group.

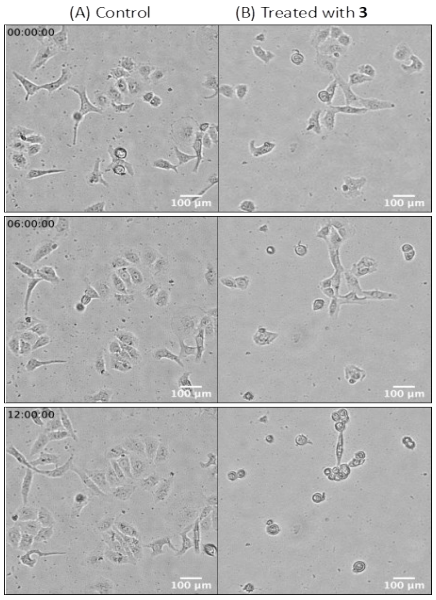

Fig. S36 Captures of the live imaging of the effect of complex **3** (10 µM) on HeLa cells at 0, 6 and 12 h.

Results and discussion

UV-Vis, FTIR and EPR spectroscopy of the complexes

In the case of square pyramidal geometry, the four d orbitals lie very close to each other making it difficult to resolve the bands to distinct Orgel components. So, the broad d→d band observed in the spectra may be assigned to $^2E_g \rightarrow {}^2T_{2g}$ transition.[28]

In the FT-IR spectra of the complexes, the C=O band shifted to a lower frequency (1630-1625 cm^{-1}) compared to that of the ligands (1642-1630 cm^{-1}), indicating the coordination of carbonyl oxygen to Cu(II) ion. The C=N band was observed around 1600-1557 cm^{-1} in the spectra of the ligands, which shifted to a lower value of 1573-1524 cm^{-1} on complexation, proving the coordination of azomethine nitrogen to Cu(II) ion. The coordination of sulphur atom of the ligand was confirmed by a band at 864-762 cm^{-1} in the spectra of complexes wherein a decrease in the group frequency was observed. The absence of N–H band around 3200 cm^{-1} in the spectrum of complex **5** indicated the coordination of sulphur as thiolato (anionic) form. The far-IR spectra of the complexes denoted the presence of coordination bonds between the donor atoms of the ligands and Cu(II) ion. The Cu–O,

Cu–N, Cu–S and Cu–Cl frequencies were observed in the ranges of 518-506, 478-440, 336-309 and 291-264 cm^{-1} respectively.[28]

The average g tensors were found using the expression, $g_{av} = (g_{\|}+2g_{\perp})/3$. The calculated g_{av} values were greater than 2, suggesting certain covalent character in the complexes.[29] The variation in the g_{av} values (Table S1) might be due to the changes in the overall geometry and the subsequent differences in the covalency of the bonds. The deviation from ideal geometry was noted from the distortion factor ($f(\alpha) = g_{\|}/A_{\|}$) which ranged 139-121 cm for the present complexes. This proposed moderately distorted geometry.[30] The degree of exchange interaction between copper centres was calculated using the following equation where G, the geometric parameter is given by

$$G = \frac{g_{\|} - 2.0023}{g_{\perp} - 2.0023}$$

If G > 4, exchange interaction is negligible and if it is less than 4, considerable exchange interaction is possible in the solid complex. The G values for complexes **1**-**4** were found to be in the range 6.29-4.12, indicating the fact that the unit cell of the compounds contained magnetically equivalent sites with negligible interaction. This insignificant interaction may lead to dissociation of dimeric complexes **3** and **4** in highly polar solvents. But, for complex **5**, the G value was found to be 2.76 and 3.89 at RT and LNT respectively. Since G < 4, exchange interaction might be present in complex **5**, which can make the dissociation of dimeric species difficult even in polar solvents.[29] The bonding parameters α^2, β^2 and γ^2 are considered as the indexes of in-plane σ bonding, in-plane π bonding and out of plane π bonding, respectively. The values of α^2 were calculated using the expression,[30] $\alpha^2 = -A_{\|}/0.036 + (g_{\|}-2.0023) + 3/7\ (g_{\perp}-2.0023) + 0.04$. With the purpose of evaluating the orbital reduction factors $K_{\|}$ and $K_{\perp}$, the following expressions were employed,

$K_{\|}^2 = (g_{\|}-2.0023)\ E / 8\lambda_0$

$K_{\perp}^2 = (g_{\|}-2.0023)\ E / 2\lambda_0$

where E is the energy of d→d transition, and λ_0 represents the spin orbit coupling constant which is –828 cm^{-1} for a free Cu(II) d^9 system. The values $K_{\|} = K_{\perp} = 0.77$ imply pure σ bonding, $K_{\|} < K_{\perp}$ suggests in-plane π bonding, and $K_{\|} > K_{\perp}$ denotes out of plane π bonding. In the present Cu(II) complexes, $K_{\|} > K_{\perp}$, signifying the presence of significant out of plane π bonding[29] in complexes **1**-**4** whereas in complex **5** ($K_{\|} < K_{\perp}$) where the sulphur is coordinated as thiolato, a significant in-plane π bonding was observed.[30] From the values of the calculated $K_{\|}$ ($= \alpha^2\beta^2$) and $K_{\perp}$ ($= \alpha^2\gamma^2$), β^2 and γ^2 were evaluated. The parameter $\alpha^2 = 1$ means complete

ionic character, while $\alpha^2 = 0.5$ signifies 100% covalent bonding. The calculated α^2 values (0.726-0.784) were lower than β^2 (0.762-1.068), representing more covalency in in-plane σ bonding than in the in-plane π bonding. In case of complex **5**, β^2 and γ^2 values were greater than 1, suggesting dominant ionic character in the π bonding when compared to the other complexes.[29] The EPR bonding parameters are tabulated (Table S2).

ESI-MS spectrometry

Mass of all the complexes was analyzed in methanol solvent. For complexes **1** and **2**, $[M–2H^+–Cl^–+CH_3OH]^+$ peaks were observed at *m/z* values of 374.9759 and 388.9284 respectively. For complex **3**, a fragment peak at *m/z* value 759.0856 may be assigned to $[M–H_2O–H^+ +CH_3OH]$, representing the binuclear structure of complex **3** as suggested and confirmed by single crystal X-ray study. Complex **4** showed a peak corresponding to $[M–2H_2O–H^+ +2CH_3OH]$ molecular ion at *m/z* 881.0370. This indicated that the complex existed as bimetallic species with two bridging chloride ions. Complexes **3** and **4** being dicationic complexes, the fragment peaks with *m/z* values corresponding to $[M+2CH_3OH–4H^+]/2$ were also observed at 402.9823 and 457.0008 respectively. For complex **5**, molecular ion peak observed at *m/z* 926.9726 corresponded to $[M+CH_3OH]$, denoting binuclear nature of complex **5**. It comprised of two bridging chloride ions around the copper centres wherein thiolato sulphur coordination was evidenced.

Thermal studies

The TGA were performed for complexes **2**, **4** and **5**, since suitable crystals were not obtained. Also, the presence of methanol adducts in the molecular ion mass peaks made it mandatory to ensure whether the chemical structure of the complexes itself contained methanol molecules or not. For complexes **2** and **4**, the initial weight loss was observed at 216°C with 17.5 and 13.58 % respectively. Similarly, for complex **5**, the initial weight loss of 8.95 % was witnessed at 209°C. As the complexes showed no observable weight loss around 80-150°C,[31] it can be confirmed that no methanol as well as water molecules were present in the coordination sphere or outside the coordination sphere.

Enzymes mimicking abilities of the complexes

Catechol oxidase-like activity

In all the samples, the product (3,5-DTBQ) was found as sodium adduct with the *m/z* value of 243.1369-243.1570 (calc. 243.1323). In the case of complex **1**, the active species was found to be $[M–2Cl^–]^{2+}$ that was obtained as molecular ion $[M–2Cl^–+CH_3OH+H_2O]^+$ with the *m/z* value of 359.0078. Hence, the active species might be in hydrated form. The association of

the active species of the complex with substrate 3,5-DTBC was witnessed at the *m/z* value of 567.2143 (calc. 567.1464), which signified $[M–2Cl^–+(3,5\text{-DTBC}–H)(H_2O)_2]^+$ ion (Fig. S14). In the reaction catalysed by complex **2**, the intermediate species was observed as sodium adduct $[M–2Cl^–+(3,5\text{-DTBC}–H)Na^+]^+$ at the *m/z* value of 567.2255 (calc. 567.1220) whereas the active species of the complex was depicted at the *m/z* value of 387.0482 that denoted the molecular ion peak $[M–2Cl^–+2CH_3OH]^+$ (Fig. S15). The binuclear Cu(II) complex (**3**) was found to dissociate into an active mononuclear species (M′) which was observed as $[M'–Cl^–+H^+]^+$ at the *m/z* value of 339.2033 (calc. 339.01). The interaction of the substrate with catalyst **3** was also observed at *m/z* = 559.3724 (calc. 559.1566) as $[M'–Cl^–+H^++(3,5\text{-DTBC}–H)]^+$ ion (Fig. S16). Finally, for complex **4**, an active monometallic species $[M'–Cl^––H]^+$ was observed at the *m/z* value of 391.0423 (calc. 391.0424) while the interaction adduct of the catalyst and substrate was found at the *m/z* value of 611.1882 (calc. 611.2036), depicting $[M'–Cl^––H+(3,5\text{-DTBC}–H)]^+$ ion (Fig. S17). The redox cycling of Cu(II) to Cu(I) was evidenced from the decrease in the d→d band with the progress of the reaction. But there was no steady decrease in the d→d band as with the progress of reaction and time, the Cu(I) species was reoxidised to Cu(II) in the presence of dioxygen[32].

In order to confirm the generation of H_2O_2 as a side product of the reaction, the modified iodometric method[33] was employed. After one hour of the reaction, the mixture was diluted with equal volume of water, and the product quinone formed was extracted using dichloromethane. The aqueous layer was then treated with diluted sulphuric acid till pH became 2, and one-third volume of 10% KI in water was added along with a few drops of ammonium molybdate solution. Due to the presence of H_2O_2 in the mixture, iodine was released, $H_2O_2 + 2I^– + 2H^+ \rightarrow 2H_2O + I_2$. The excess iodide ions facilitated the formation of triiodide ions. The ammonium molybdate solution promoted this slow reaction to become instantaneous.[33] A band characteristic of $I_3^–$ ion was detected at 353 nm and monitored spectrophotometrically (Fig. S18), indicating the formation of H_2O_2 as a side product. The control experiments were done using commercial H_2O_2 in the absence of the catalyst and 3,5-DTBC in order to confirm the formation of $I_3^–$ spectrophotometrically at 353 nm.

Further, the inactivity of complex **5** can be explained due to the anionic coordination of S to Cu(II) ion. Here, the monocationic active species (less positive) might be generated, which had less tendency to interact with the anionic substrate.[34]

Binding of the complexes with biomolecules

Complex-DNA interactions

DNA is considered as an important intracellular target for many anticancer drugs. Mostly, cytotoxicity of anticancer drugs is associated with their ability to bind with DNA either covalently or non-covalently. The non-covalent interactions which arise *via* intercalative, groove or electrostatic binding are of main interest since they induce less toxicity and interfere with the normal DNA functions including DNA replication and protein interaction.[12] The interactions of the complexes (**1**-**5**) with CT DNA were examined by absorption titration, ethidium bromide displacement and viscosity methods. The results clearly indicated a strong intercalative mode of interaction between the two.

The interactions between the complexes and CT-DNA were studied using UV-Vis absorption spectroscopy by noting down the changes in the absorbance of the complexes. To a fixed concentration of the complexes (20 μM) in Tris-HCl buffer, CT-DNA solution (0-50 μM) was added stepwise, resulting in a decrease in the absorbance (hypochromism) of the intraligand transitions at 282-286 and 293-323 nm. The magnitudes of the hypochromism (18-29%) and red shift (1-3 nm) were measured, which revealed the intercalative mode of interaction between the complexes and CT-DNA (Fig. S21). This might be due to the stacking of the aromatic chromophores of the complexes with the base pairs of CT-DNA.[11] The intrinsic DNA binding constants (K_b) and apparent DNA binding constants (K_{app}) of the complexes were evaluated using equations S1 and S2, and found in the order **3** > **4** > **5** > **2** > **1**. The free uncomplexed ligands exhibited 10^2 times lesser binding affinity than the present complexes[35].

Fluorescence emission spectroscopy was also used to find the interactions between the complexes and DNA. Ethidium bromide (EB) was used as fluorophore which when bound to CT-DNA displayed greater fluorescence due to its strong interaction with the neighbouring DNA base pairs. When the complexes (0-45 μM) were added incrementally to a fixed concentration of EB-DNA (5 μM), the displacement of EB from the DNA base pairs occurred due the effective competition of the complexes with EB, resulting in the quenching of the emission intensity. The relative strength of the interactions between the complexes and CT-DNA was interpreted from the extent of fluorescence quenching.[12] The fluorescence emission spectra of EB-DNA with and without the complexes are shown in Fig. S22. The apparent DNA binding constants (K_{app}) and quenching constants (K_{sv}) were calculated, and the trend was in the order **3** > **4** > **5** > **2** > **1**. The K_b, K_{sv} and K_{app} values are provided in Table S6.

Viscosity of CT-DNA was measured for further studying the interactions of the complexes with DNA. The DNA viscosity is said to increase when a complex intercalates into the DNA base pairs, due to the lengthening and stiffening of the DNA double helix. The

addition of different concentrations of the complexes (0-75 μM) to CT-DNA (100 μM) led to an increase in the viscosity of CT-DNA, confirming the intercalative mode of binding. In addition, the plot of relative viscosity *vs* [complex]/[DNA] (Fig. S23) revealed that the ability of the complexes to increase the viscosity of CT-DNA depends upon the substitution on the terminal *N* of the ligand as well as the nuclearity of the complexes. The ability of the complexes to increase the viscosity followed the order **3** > **4** > **5** > **2** > **1**, which was in accordance with the results obtained from the spectroscopic studies. Thus, it can be said that complex **3** having ethyl as terminal *N* substituent has enhanced binding ability compared to the other complexes.[36]

Complex-BSA protein interactions

Many anticancer drugs depend on their interaction with serum albumin, a major transport protein in blood, for their activity and metabolism.[14] The affinity of the Cu(II) complexes with the protein was examined by emission spectroscopy utilising the fluorescence property of BSA (bovine serum albumin). The amino acid residues in BSA, namely tryptophan, tyrosine and phenylalanine are mainly responsible for intrinsic protein fluorescence. Among the five complexes, complex **3** was able to bind with BSA more strongly than the other complexes.

The variations in the BSA fluorescence intensity were noted over the range of 285-450 nm with the incremental addition of the complexes (0-30 μM) to a fixed concentration of BSA (1 μM) prepared in PBS buffer solution (pH = 7.2). The quenching of BSA fluorescence (Fig. S24) with the addition of the complexes was observed at λ = 346 nm with the percentage of 74.95-91.87% (Fig. S25) along with a bathochromic shift of 1-10 nm. In order to find the type of quenching caused by the complexes on BSA, the UV-Vis absorbance of BSA with an equal concentration of the complex was monitored. Various considerable changes in the UV-Vis spectra were noted upon addition of the complexes to BSA due to the formation of new compounds between the quenchers and BSA. This denoted a static quenching mechanism. The probability of the dynamic quenching was neglected since that affects only the excited-state fluorescent molecule without influencing the contour of UV-Vis spectra. The K_b, K_q and *n* (no. of binding sites) values are provided in Table S7.

The synchronous emission spectra on the addition of the Cu(II) complexes to BSA are shown in Fig. S26. The decline in the emission intensities of the spectra at both the wavelengths (302 and 343 nm) with slight blue shift (2-5 nm) was found. Hence, it was confirmed that the binding of both the protein residues had occurred simultaneously.[11]The

complexes were able to induce conformational changes in the tyrosine as well as the tryptophan microenvironments.

The comparison of the DNA and BSA binding of the complexes revealed that the complexes had more affinity towards DNA except complex **3** which showed more interaction with BSA. The present Cu(II) complexes exhibited almost thrice the value of DNA/protein binding constants when compared to the similar mononuclear Cu(II) chromone TSC complexes.[36]

Molecular docking studies

Ligand efficiency (LE) is referred as the magnitude of virtuousness of interaction of a compound with its target protein. It is the measurement of the binding affinity per atom of a complex with its binding protein.[37] Complexes **1** and **3** displayed significant binding with CASP3 protein with a LE value of -0.264 and -0.106 respectively. The lower LE of complex **3** compared to complex **1** can be explained based on the concept of size dependency. When a small compound binds to the active sites of protein, LE is high. On the other hand, large compounds bind not only to the active sites but also to other moieties of protein, decreasing the value of LE.[38] The study proposed that both the Cu(II) complexes had considerable binding affinity with the target protein with a better LE, which may facilitate apoptotic mode cell death in the anticancer assay. The Pymol and Ligplot representation of docking poses of complexes are provided in Figs. S29-S32.

Complex	Room temperature data				Liquid nitrogen temperature data					
	$g_{\parallel}$	$g_{\perp}$	G	g_{av}	$g_{\parallel}$	$g_{\perp}$	G	$A_{\parallel}$ [a]	g_{av}	f [b] (cm)
1	2.222	2.055	4.168	2.110	2.225	2.052	4.472	160	2.109	139
2	2.216	2.054	4.133	2.108	2.199	2.039	5.315	181	2.092	121
3	2.213	2.050	4.417	2.104	2.190	2.032	6.298	172	2.084	127
4	2.207	2.052	4.124	2.105	2.188	2.035	5.637	177	2.086	123
5	2.145	2.054	2.760	2.054	2.392	2.114	3.488	174	2.026	137

Table S1. EPR parameters of the Cu(II) complexes

[a] $A_{\parallel}$ values are denoted in Gauss (G).

[b] Parameter $f = g_{\parallel}/A_{\parallel}$.

Table S2. EPR bonding parameters of the Cu(II) complexes

Complex	α^2	β^2	λ^2	$K_{\parallel}$	$K_{\perp}$
1	0.7260	0.7623	0.7469	0.5535	0.5422
2	0.7770	0.8814	0.8660	0.6848	0.6730
3	0.7481	0.9317	0.8800	0.6969	0.6583
4	0.7572	0.9608	0.9468	0.7273	0.7168
5	0.7842	1.068	1.285	0.8376	1.008

Table S3. Selected bond lengths (Å) and angles (°) of complexes **1** and **3**

	1	**3**
Cu(1)–Cl(1)	2.2656(8)	2.2817(6)
Cu(1)–Cl(2)/Cl(1)#1	2.5719(8)	2.6726(7)
Cu(1)–S(1)	2.2692(8)	2.2448(7)
Cu(1)–O(1)	1.9892(19)	1.9712(17)
Cu(1)–N(1)	2.010(2)	1.981(2)
S(1)–C(11)	1.698(3)	1.709(3)
O(1)–C(3)	1.249(3)	1.259(3)
N(1)–N(2)	1.383(3)	1.381(3)
N(1)–C(1)	1.285(4)	1.287(3)
N(2)–H(2)	0.88	0.88
N(2)–C(11)	1.344(4)	1.354(3)
N(3)–H(3A)	0.88	0.88
Cl(1)–Cu(1)–Cl(2)/Cl(1)#1	98.20(3)	96.38(2)
Cl(1)/Cl(1)#1–Cu(1)–S(1)	91.00(3)	98.54(2)
S(1)–Cu(1)–Cl(2)/Cl(1)	99.59(3)	90.52(2)
O(1)–Cu(1)–Cl(1)/Cl(1)#1	91.06(6)	87.39(5)
O(1)–Cu(1)–Cl(2)/Cl(1)	90.06(6)	90.43(5)
O(1)–Cu(1)–S(1)	169.74(6)	173.85(6)
O(1)–Cu(1)–N(1)	89.72(9)	91.60(8)
N(1)–Cu(1)–Cl(1)	167.15(7)	169.91(6)
N(1)–Cu(1)–Cl(2)/Cl(1)#1	94.62(7)	93.59(6)
N(1)–Cu(1)–S(1)	86.06(7)	86.44(6)
C(11)–S(1)–Cu(1)	96.93(11)	97.10(9)
C(3)–O(1)–Cu(1)	128.89(18)	126.65(16)
Cu(1)–Cl(1)–Cu(1)#1	NA	83.62(2)

Symmetry transformations used to generate equivalent atoms: #1 -x, -y+1, -z+1.

NA = Not applicable.

Table S4. Previously reported K_{cat} values for the oxidation of DTBC catalysed by the Cu(II) complexes

Complex	**Solvent**	K_{cat} **(h^{-1})**	**Ref.**
$[Cu_2(H_2\text{-bbppnol})(\mu\text{-OAc})(H_2O)_2]Cl_2{\cdot}2H_2O$ H_2-bbppnol = *N*,*N'*-bis(2-hydroxybenzyl)-*N*,*N'*-bis-(pyridylmethyl)]-2-hydroxy-1,3-propanediamine	CH_3OH saturated with O_2	28	39
[Cu(L)] H_2L = 2,2'-{cyclohexane-1,2 diylbis[nitrilo(1*E*)eth-1-yl-1-ylidine]}bis[5-(prop-2-yn-1-yloxy)phenol]	CH_3CN	150	32
[Cu(L)] H_2L = *N*-(*N'*,*N'*-diethylaminothiocarbonyl)benzimidoyl chloride-2-aminoacetophenone-*N*-methylthiosemicarbazone	DMSO	146	40
$[CuL(NO_3)(H_2O)]{\cdot}H_2O$ HL = (*E*)-*N'*-(2-hydroxy-5-methylbenzylidene)benzohydrazide	CH_3OH / 0.02 M HEPES medium, pH = 8.0, 25 °C.	1.45×10^4	41
$[Cu(\mu\text{-Cl})(HL3)]_2Cl_2$ HL3 = 4-oxo-4H-chromene-3-carbaldehyde-4(*N*)-ethylthiosemicarbazone	CH_3OH	256	This work

Table S5. Previously reported K_{cat} values for the hydrolysis of phosphates catalysed by the Cu(II) complexes

Complex	Solvent	K_{cat} (h^{-1})	Ref.
$[Cu_5(tdciH_{-2})(tdci)_2(OH)_2(NO_3)_2](NO_3)_4 \cdot 6H_2O$ tdci = 1,3,5-trideoxy-1,3,5-tris(dimethylamino)-*cis*-inositol	0.02 M buffer (HEPES and CHES)	28	42
[Cu(L)] H_2L = 2,2'-{cyclohexane-1,2 diylbis[nitrilo(1*E*)eth-1-yl-1-ylidine]}bis[5-(prop-2-yn-1-yloxy)phenol]	CH_3CN	114	32
[Cu(L)] H_2L = *N*-(*N'*,*N'*-diethylaminothiocarbonyl)benzimidoyl chloride-2-aminoacetophenone-*N*-methylthiosemicarbazone	DMSO	5080	40
$[Cu_2(\mu\text{-}CH_3COO)(\mu\text{-}H_2O)(\mu\text{-}OH)(phen)_2]^{2+}$ phen = 1,10-phenanthroline	CH_3CN-water medium (2.5% (*v*/*v*))	12.4	43
$[Cu(\mu\text{-}Cl)(HL3)]_2Cl_2$ HL3 = 4-oxo-4H-chromene-3-carbaldehyde-4(*N*)-ethylthiosemicarbazone	97.5:2.5 (*v*/*v*) DMF-H_2O	642	This work

Table S6. DNA binding parameters for the Cu(II) complexes

Complex	K_b (M^{-1})	K_q (M^{-1})	K_{app} (M^{-1})
1	3.03×10^6	3.38×10^4	1.11×10^6
2	3.86×10^6	3.52×10^4	1.16×10^6
3	6.92×10^6	6.90×10^4	1.56×10^6
4	6.51×10^6	4.22×10^4	1.31×10^6
5	6.20×10^6	3.95×10^4	1.28×10^6

Table S7. BSA binding parameters for the Cu(II) complexes

Complex	K_b (M^{-1})	K_q (M^{-1})	*n*
1	1.51×10^6	1.41×10^5	0.926
2	2.16×10^6	2.62×10^5	1.026
3	1.42×10^7	3.10×10^5	0.939
4	5.40×10^6	3.09×10^5	0.869
5	5.06×10^6	2.95×10^5	0.812

Table S8. IC_{50} values for the antioxidant activity of the Cu(II) complexes

Compound	IC_{50} (μM)	
	DPPH	**ABTS**
1	4.18	48.91
2	4.04	31.18
3	3.55	7.92
4	3.92	11.85
5	6.36	46.98
Ascorbic acid	6.99	41.94
Gallic acid	3.24	8.07

Table S9. Anti-haemolytic activity of the Cu(II) complexes against H_2O_2 induced haemolysis

Control / Complex (1000 μg/mL)	Optical density at 540 nm	% inhibition of haemolysis
Positive control	1.040	NA
Negative control	0.027	NA
1	0.046	95.57
2	0.045	95.67
3	0.044	95.73
4	0.040	96.08
5	0.036	96.50

Table S10. Molecular docking and ligand efficiency parameters for Cu(II) complexes **1** and **3** with CASP3 protein, VEGFR2 and PIM-1 kinase receptors

Receptor	Complex	Docking score (kcal/mol)	Glide energy (kcal/mol)	Ligand efficiency	Hydrogen bonding interaction(s)	Hydrophobic interactions
CASP3	**1**	-4.45	-31.65	-0.264	Gly122	Phe256, Trp206, Tyr204, His121, Cys163, Ser205
	3	-5.27	-45.24	-0.106	Arg164	Gly60, Met61, His121, Tyr204, Cys163, Ser205, Arg207, Trp206, Phe250, Ser251, Phe256, Phe252, Asp253
VEGFR2	**1**	-6.30	-26.33	-0.315	Asn921	Gly920, Cys917, Ala864, Phe1045, Val914, Glu915, Val897, Leu1033, Phe916, Leu838
	3	-7.94	-45.24	-0.189	Arg840 Cys917	Val914, Phe1045, Val846, Val897, Ala864, Glu915, Leu1033, Glu848, Gly920, Lys918, Lys836, Asn921,Leu838, Lys866
PIM-1	**1**	-7.62	-37.68	-0.381	Asp131	Phe49, Ile185, Ala65, Leu174, Val126
	3	-7.69	-74.97	-0.183	Asp186 Asp131	Lys169, Asp167, Glu171, Phe130, Asp128, Leu174, Asn172, Ile185, Phe49

References

[1] APEX3 "Program for data collection on area detectors" BRUKER AXS Inc., 5465 East Cheryl Parkway, Madison, WI 53711-5373 USA.

[2] G. M. Sheldrick, *Acta Crystallogr. Sect. A Found. Crystallogr.*, 2008, **64**, 112–122.

[3] G. M. Sheldrick, *Acta Crystallogr. Sect. A Found. Crystallogr.*, 2015, **71**, 3–8.

[4] G. M. Sheldrick, *Acta Crystallogr. Sect. C Struct. Chem.*, 2015, **71**, 3–8.

[5] SADABS, G. M. Sheldrick, "Program for absorption correction of area detector frames", BRUKER AXS Inc., 5465 East Cheryl Parkway, Madison, WI 53711-5373 USA.

[6] A. L. Spek, *J. Appl. Crystallogr.*, 2003, **36**, 7–13.

[7] O. V. Dolomanov, L. J. Bourhis, R. J. Gildea, J. A. K. Howard and H. Puschmann, *J. Appl. Crystallogr.*, 2009, **42**, 339–341.

[8] J. A. Glasel, *Biotechniques*, 1995, **18**, 62–63.

[9] A. M. Pyle, J. P. Rehmann, R. Meshoyrer, N. J. Turro, J. K. Barton and C. V. Kumar, *J. Am. Chem. Soc.*, 1989, **111**, 3051–3058.

[10] K. S. Ghosh, B. K. Sahoo, D. Jana and S. Dasgupta, *J. Inorg. Biochem.*, 2008, **102**, 1711–1718.

[11] J. Haribabu, K. Jeyalakshmi, Y. Arun, N. S. P. Bhuvanesh, P. T. Perumal and R. Karvembu, *RSC Adv.*, 2015, **5**, 46031–46049.

[12] J. Haribabu, K. Jeyalakshmi, Y. Arun, N. S. P. Bhuvanesh, P. T. Perumal and R. Karvembu, *J. Biol. Inorg. Chem.*, 2017, **22**, 461–480.

[13] M. R. Eftink, Topics in fluorescence spectroscopy, Volume 6: Protein fluorescence, Kluwer Academic / Plenum Publishers, New York, 2000.

[14] N. Balakrishnan, J. Haribabu, D. Anantha Krishnan, S. Swaminathan, D. Mahendiran, N. S. P. Bhuvanesh and R. Karvembu, *Polyhedron*, 2019, **170**, 188–201.

[15] G. U. Bae, D. W. Seo, H. K. Kwon, H. Y. Lee, S. Hong, Z. W. Lee, K. S. Ha, H. W. Lee and J. W. Han, *J. Biol. Chem.*, 1999, **274**, 32596–32602.

[16] B. L. Halvorsen, K. Holte, M. C. W. Myhrstad, I. Barikmo, E. Hvattum, S. F. Remberg, A.-B. Wold, K. Haffner, H. Baugerød, L. F. Andersen, Ø. Moskaug, D. R. Jacobs and R. Blomhoff, *J. Nutr.*, 2002, **132**, 461–471.

[17] M. N. Alam, N. J. Bristi and M. Rafiquzzaman, *Saudi Pharm. J.*, 2013, **21**, 143–152.

[18] N. P. Seeram, S. M. Henning, Y. Niu, R. Lee, H. S. Scheuller and D. Heber, *J. Agric. Food Chem.*, 2006, **54**, 1599–1603.

[19] I. Parejo, F. Viladomat, J. Bastida, A. Rosas-Romero, N. Flerlage, J. Burillo and C. Codina, *J. Agric. Food Chem.*, 2002, **50**, 6882–6890.

[20] T. Afsar, S. Razak, M. R. Khan, S. Mawash, A. Almajwal, M. Shabir and I. U. Haq,

BMC Complement. Altern. Med., 2016, **16**, 258.

[21] M. Naim, B. Gestetner, A. Bondi and Y. Birk, *J. Agric. Food Chem.*, 1976, **24**, 1174–1177.

[22] D. Lee, S. A. Long, J. L. Adams, G. Chan, K. S. Vaidya, T. A. Francis, K. Kikly, J. D. Winkler, C. M. Sung, C. Debouck, S. Richardson, M. A. Levy, W. E. DeWolf, P. M. Keller, T. Tomaszek, M. S. Head, M. D. Ryan, R. C. Haltiwanger, P. H. Liang, C. A. Janson, P. J. McDevitt, K. Johanson, N. O. Concha, W. Chan, S. S. Abdel-Meguid, A. M. Badger, M. W. Lark, D. P. Nadeau, L. J. Suva, M. Gowen and M. E. Nuttall, *J. Biol. Chem.*, 2000, **275**, 16007–16014.

[23] G. Madhavi Sastry, M. Adzhigirey, T. Day, R. Annabhimoju and W. Sherman, *J. Comput. Aided. Mol. Des.*, 2013, **27**, 221–234.

[24] Schrödinger Release 2015-1: MacroModel, Schrödinger, LLC, New York, NY, 2015.

[25] Schrödinger Release 2015-1: Glide, Version 6.6, Schrödinger, LLC, New York, NY, 2015

[26] K. Jeyalakshmi, J. Haribabu, C. Balachandran, E. Narmatha, N. S. P. Bhuvanesh, S. Aoki, S. Awale and R. Karvembu, *New J. Chem.*, 2019, **43**, 3188–3198.

[27] S. Kasibhatla, *Cold Spring Harb. Protoc.* 2006, 2006, **3**, pdb.prot4493.

[28] P. F. Rapheal, E. Manoj and M. R. Prathapachandra Kurup, *Polyhedron*, 2007, **26**, 818– 828.

[29] P. Murali Krishna, K. Hussain Reddy, J. P. Pandey and D. Siddavattam, *Transition Met. Chem.*, 2008, **33**, 661–668.

[30] R. C. Chikate, A. R. Belapure, S. B. Padhye and D. X. West, *Polyhedron*, 2005, **24**, 889–899.

[31] N. Kavitha and P. V. Anantha Lakshmi, *J. Saudi Chem. Soc.*, 2017, **21**, S457–S466.

[32] C. Balakrishnan, M. Theetharappan, P. Kowsalya, S. Natarajan, M. A. Neelakantan and S. S. Mariappan, *Appl. Organomet. Chem.*, 2017, **31**, e3776.

[33] S. K. Dey and A. Mukherjee, *New J. Chem.*, 2014, **38**, 4985–4995

[34] T. Chakraborty, S. Mukherjee, S. Dasgupta, B. Biswas and D. Das, *Dalton Trans.*, 2019, **48**, 2772–2784.

[35] Y. Li, Z. Y Yang and J. C. Wu, *Eur. J. Med. Chem.*, 2010, **45**, 5692–5701.

[36] G. Kalaiarasi, S. R. J. Rajkumar, S. Dharani, V. M. Lynch and R. Prabhakaran, *Inorg. Chim. Acta*, 2018, **471**, 759–776.

[37] P. W. Kenny, *J. Cheminform.*, 2019, **11**, 8.

[38] M. Orita, K. Ohno, M. Warizaya, Y. Amano and T. Niimi, *Lead Generation and Examples: Opinion Regarding How to Follow up Hits*, Elsevier Inc., 1st Edn., 2011, Vol. 493.

[39] A. Neves, L. M. Rossi, A. J. Bortoluzzi, B. Szpoganicz, C. Wiezbicki, E. Schwingel, W. Haase and S. Ostrovsky, *Inorg. Chem.*, 2002, **41**, 1788–1794.

[40] P. Vijayan, P. Viswanathamurthi, K. Velmurugan, R. Nandhakumar, M. D. Balakumaran, P. T. Kalaichelvan and J. G. Malecki, *RSC Adv.*, 2015, **5**, 103321–103342.

[41] S. Anbu, A. Paul, A. P. C. Ribeiro, M. F. C. Guedes da Silva, M. L. Kuznetsov and A. J. L. Pombeiro, *Inorg. Chim. Acta*, 2016, **450**, 426–436.

[42] T. Gajda, Y. Düpre, I. Török, J. Harmer, A. Schweiger, J. Sander, D. Kuppert and K. Hegetschweiler, *Inorg. Chem.*, 2001, **40**, 4918–4927.

[43] S. Anbu, M. Kandaswamy, S. Kamalraj, J. Muthumarry and B. Varghese, *Dalton Trans.*, 2011, **40**, 7310–7318.